In-depth description of Electrohydrodynamic conduction pumping of dielectric liquids: physical model and regime analysis

P.A. Vázquez,[1] M. Talmor,[2] J. Seyed-Yagoobi,[2] P. Traoré,[3] and M. Yazdani[4]
[1)]*Departamento de Física Aplicada III, Universidad de Sevilla, ETSI, Camino de los Descubrimientos s/n, 41092 Sevilla, Spain.*[a)]
[2)]*Multi-Scale Heat Transfer Laboratory, Department of Mechanical Engineering, Worcester Polytechnic Institute, Worcester, MA 01609, USA.*
[3)]*Institut PPRIME, Département Fluide-Thermique-Combustion, Boulevard Pierre et Marie Curie, BP 30179, 86962 Futuroscope-Chasseneuil, France.*
[4)]*United Technologies Research Center, East Hartford, CT 06108, USA.*

(Dated: 18 October 2019)

In this work we discuss fundamental aspects of Electrohydrodynamic (EHD) conduction pumping of dielectric liquids. We build a mathematical model of conduction pumping that can be applied to all sizes, down to micro-sized pumps. In order to do this, we discuss the relevance of the Electrical Double Layer (EDL) that appears naturally on non-metallic substrates. In the process we identify a new dimensionless parameter, related to the value of the zeta potential of the substrate-liquid pair, that quantifies the influence of these EDLs on the performance of the pump. This parameter also describes the transition from EHD conduction pumping to electroosmosis. We also discuss in detail the two limiting working regimes in EHD conduction pumping: ohmic and saturation. We introduce a new dimensionless parameter, accounting for the electric field enhanced dissociation, that along with the conduction number, allows to identify in which regime the pump operates.

I. INTRODUCTION

The future of fluidic heat transfer systems lies in innovative solutions for fluid flow generation and control that can address the evolving needs of modern high power systems, both terrestrially and in space. Traditional mechanical pumping techniques, although efficient and well understood, are difficult to miniaturize and suffer from mechanical breakdown, excessive vibrations, and difficulty with pumping thin liquid films and multi-phase flows. As an active method for flow control in fluidic heat transfer systems, Electrohydrodynamic (EHD) conduction pumping[1–6] has unique advantages over traditional, mechanical methods for generation of flow. EHD conduction pumps have simple, compact designs with no moving parts and therefore low vibrations and acoustic noise. These pumps have been shown to enhance heat transfer at different size scales, ranging from cm[7,8], mm[9] to hundreds of μm[10] and in the presence and absence of gravity[11]. It has been shown to enhance significantly the heat transfer in pool boiling systems[11,12].

EHD flows are generated by electric forces acting on electric charges present in a liquid[13]. There are three main mechanisms to generate a net volumetric electric charge in a liquid: injection, induction and conduction[14]. In the first case electric charges are injected from the electrodes into the liquid. The induction mechanism of charge generation is based in the existence of a gradient or discontinuity of the electrical conductivity. In conduction the charges are generated by dissociation of a weak electrolyte in the liquid. The last one is the mechanism used in EHD conduction pumping.

Under equilibrium conditions, with no applied electric field or under the effect of only a weak electric field (less than $10^6\,\mathrm{V/m}$, in order to not affect the dissociation process), the electrolyte impurities found within a dielectric liquid undergo reversible dissociation and recombination reactions at equal rates. These reactions are described as,

$$AB \underset{\text{rec.}}{\overset{\text{dis.}}{\rightleftharpoons}} A^+ + B^-. \tag{1}$$

where AB is a simple neutral electrolyte species, while A^+ and B^- are the positive and negative ions it dissociates into. The bulk of the liquid, in equilibrium, is electroneutral, but near a surface this equilibrium breaks, due to the presence of the interface. As a consequence, near a surface an Electric Double Layer (EDL) develops[15]. This is true independently of the application of an external electric field, or whether the surface is metallic or dielectric. The simplest structure of an EDL is comprised of a layer of ions stuck on the interface (the Stern layer) and a diffuse layer in the liquid (the Debye layer), with a net electric charge. The thickness of the diffuse layer, the Debye length λ_D, is determined by the equilibrium between charge diffusion and recombination. The typical diffusion time is $\tau_D = \lambda_D^2/D$, while the typical recombination time is $\tau_\sigma = \varepsilon/\sigma$. Here, D is the diffusion coeficient, ε is the permittivity and σ is the electrical conductivity. In equilibrium $\tau_D \approx \tau_\sigma$, and we get, for the case of a univalent symmetric electrolyte with equal ionic mobilities for both species[15,16]

$$\lambda_D = \sqrt{\frac{\varepsilon D}{\sigma}} = \sqrt{\frac{\varepsilon K k_B T}{\sigma e_0}}. \tag{2}$$

We have used the Einstein relation $D = K k_B T/e_0$[17], where e_0 is the elementary charge, K is the ionic mobility, k_B is the Boltzmann constant and T is the absolute temperature. The electroosmosis pumps, another type of EHD pump, operate applying an electric field parallel to the surface to exert an

[a)]Electronic mail: pvazquez@us.es.

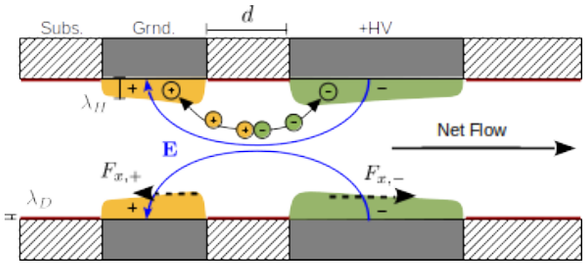

FIG. 1. Illustration of the EHD conduction mechanism. The heterocharge layers locations are indicated in green and yellow. The corresponding polarity with respect to the electrodes is shown. The placement of the EDL on the substrate is indicated with red lines.

electrical force on the EDL near the electrodes, putting the liquid into motion[14].

The charge distribution in the EDL is a result of the equilibrium between charge diffusion and ion recombination. When an electric potential is applied between metallic electrodes immersed in an electrolyte, this equilibrium is perturbed. The applied electric field, perpendicular to the electrodes, pushes away the ions of the same polarity than the electrode. Then, some of the ions of the opposite polarity do not find a counter-ion to recombine before arriving at the electrode. If the applied electric field is high enough, the Debye layer disappears and a heterocharge layer develops, with a net electric charge of opposite polarity to the electrode. The thickness of this heterocharge layer can be estimated as follows. The typical ionic velocity is KE_0, E_0 being the order of magnitude of the component of the electric field perpendicular to the surface. Then, before recombining the ions typically travel a distance

$$\lambda_H \sim KE_0\tau_\sigma = \frac{\varepsilon KE_0}{\sigma}. \tag{3}$$

Let us stress that the EDL and the heterocharge layer have fundamentally different physical origins. The EDL is the result from equilibrium between ionic diffusion and recombination, while the heterocharge layers arise from the balance between recombination and the ionic electric drift created by an external electric field. The heterocharge layers appear only next to metallic electrodes where an applied electric potential, producing a normal electric field, exists. The EDL appears in equilibrium conditions next to any solid surface in contact with an electrolyte, metallic or not.

In EHD conduction pumping, an electric field is applied across two electrodes immersed in the liquid, generating Coulomb forces acting on the heterocharge layers that develop.[1,14]. Since the force applied on the fluid is proportional to the size of the layers, and the layers form near the electrode surfaces, a simple way of affecting the size of each layer is by controlling the geometry of the electrodes used. As shown by Yazdani and Seyed-Yagoobi[18], under the assumption of equal ionic mobilities, the force for flush electrodes as shown in Figure 1 will always be directed toward the electrode with the larger wetted surface area. In this figure, a sample neutral electrolyte is shown dissociating into negative and positive ions, which drift toward the heterocharge layers over the positively charged high voltage electrodes and the ground electrodes, respectively. The electric force and the subsequent flow and pressure generations can be controlled by varying the potential applied to the electrodes.

As a promising fluid flow control technique, EHD conduction pumping has been rigorously investigated by various researchers over the past few decades. Atten and Seyed-Yagoobi[1] have formulated the initial theoretical models describing the phenomenon and its characteristic parameters, and have compared experimental results with approximate theoretical estimates for predicting pressure generation capabilities. Dimensional numerical calculations of EHD conduction in a channel were performed by Jeong, Seyed-Yagoobi, and Atten[19], for a hollow tube high voltage electrode and ring ground electrode configuration, which provided a prediction of the force distribution and pressure generation capabilities of EHD conduction pumping for certain electrode geometries. Additional fundamental nondimensional numerical studies performed by Yazdani and Seyed-Yagoobi[20,21] have shown the profiles of the heterocharge layers over flush electrodes in thin film flows driven by EHD conduction, the heat transfer enhancement potential of the EHD conduction pumping technology, and the effect of different charge mobility ratios on the characteristic parameters and performance of the EHD conduction mechanism. Mahmoudi, Adamiak, and Castle[22] were able to predict pressure generation of a macro-scale EHD conduction pump using a similar nondimensional simulation model. Experimental studies by Jeong and Seyed-Yagoobi[7] have shown the effect of electrode geometry on pressure generation in more detail, with numerical models from Feng and Seyed-Yagoobi[23] showing the profiles of the heterocharge layers in perforated electrode geometries. Experimental studies by Mahmoudi *et al.*[24] and Gharraei *et al.*[25] have also shown the effect of different working fluids on pressure generations, and experimental studies by Abe *et al.*[26] showed the effect of the surface characteristics of the electrodes on the pressure generation performance of an EHD conduction pump. It should be noted that the traditional efficiency of EHD conduction pumps in terms of flow generation (defined as the flow power generated divided by the input electric power) is very small since the transmission of electrical energy into pressure is not direct, but passes through the chemical reaction. In most cases, the traditional efficiencies recorded for EHD conduction pumps have been less than 5%, often even less than 1%[14]. However, when considering the total power consumption of these devices, which is on the order of single watts or less, this traditional formulation of efficiency becomes less relevant. When used in heat transfer applications, it is better to consider the efficiency of EHD conduction pumps in terms of heat transfer enhancement versus their input electric power. Past experiments have shown that a single watt of input power can generate two or three order of magnitudes enhancements in the resultant heat transport capacity[11,27]. Therefore, EHD conduction pumping efficiency in heat transport systems is defined as the ratio of the maximum additional heat removed from the system due to the presence of the EHD conduction pump and the input electric power to the pump.

However, the effect of the operating regime on the efficiency of EHD conduction pumps has not been investigated. There are two regimes: ohmic and saturation. In the former case the ions have time to recombine inside the volume, and an electroneutral bulk is generated. In the latter case the ions reach the electrodes before they have time to recombine. Typically these regimes are characterized for the non-dimensional conduction number, usually named C_0 in the literature[1]. In this paper we analyze in detail the dependence of the generated pressure on C_0. The application of an external electric field enhances the dissociation of electrolytes, this is the Onsager-Wien effect[13,28]. We introduce a new non-dimensional number, that we will call β, that, along with C_0, allows the characterization of the regime where a given EHD conduction pump will operate.

Another point with interesting technology applications is EHD conduction pumping in systems of micro scale, down to some tens of μm. Typically, in these geometries there is a non-conducting substrate. As it is the case for all surfaces immersed in a liquid, an EDL develops near this substrate. In macro-sized systems this EDL can be safely ignored. However, if we want to work with smaller conduit sizes, its influence could be important. In this work, we build a model of EHD conduction pumping that includes boundary conditions suited to pumps of all sizes, down to tens of microns. As a result of this analysis we introduce a new dimensionless parameter: the ratio between the natural electric field inside the double layer and the applied field between the electrodes. This parameter can also be used to describe the transition from an EHD conduction pumping to electroosmosis, where the pressure head is generated by the electric force on the EDL.

The reminder of this paper is organized as follows. In Section II, we present the physical model. We describe the physical mechanisms involved and write down the non-dimensional equations and associated boundary conditions. We also define the non-dimensional parameters relevant for the problem. The model includes the enhancement of the dissociation process induced by the applied electric field, the Onsager-Wien effect. In Section III, we discuss the two limit regimes in EHD conduction pumping: the ohmic regime and the saturation regime. We discuss in particular the generated pressure in each regime. Finally, in Section IV, we summarize the main conclusions of this work.

II. PHYSICAL MODEL

In this section we present the physical model for EHD conduction pumps. The relevant magnitudes are the ionic species concentrations, the electric potential, the electric field and the velocity and pressure fields. In the usual experimental conditions, the Joule heating can be neglected, as the electric currents are very small. As there are no heat sources or sinks in the experiments, the liquid can be assumed to be isothermal. We present the dimensional and non-dimensional equations of the model, the boundary conditions and the non-dimensional parameters. In general, we will consider boundary conditions for three types of surfaces: positive electrodes, negative electrodes and non-metallic substrates. We give the boundary conditions associated to each one of these types. The application of the model to micro-sized pumps requires an special care with the formulation of the electric boundary conditions on non-metallic substrates. The main novelty introduced here compared to previous works is the definition of two new dimensionless parameters related to the Onsager-Wien effect and the description of the EDL on non-metallic substrates, respectively.

A. Dissociation - recombination

The only source of ions in the liquid are the dissociation-recombination processes of the electrolytes present in the volume. The applied electric fields in EHD conduction pumping are never high enough to produce charge injection from the electrodes. We consider a simple model consisting of a reversible process of dissociation and recombination of a neutral species into univalent positive and negative ions[1]. In equilibrium we have

$$k_D c_0 = k_R n_+^{\mathrm{eq}} n_-^{\mathrm{eq}} = k_R \left(n_{\mathrm{eq}}\right)^2, \tag{4}$$

where c_0 is the concentration of the neutral species, n_+^{eq} and n_-^{eq} are the concentration of the positive and negative species in equilibrium (electroneutrality implies $n_+^{\mathrm{eq}} = n_-^{\mathrm{eq}} = n_{\mathrm{eq}}$). Their dimensions are m^{-3}. The dielectric liquids used in EHD conduction pumping are non-polar or weakly polar. Then, the electrolyte is weakly dissociated and the concentration of the neutral species, c_0, can be considered constant. The magnitudes k_D and k_R are the rates of dissociation and recombination, respectively. When an external electric field, $\mathbf{E}$, is applied, the rate of dissociation increases, this is the electric field enhanced dissociation effect, or Onsager-Wien effect[28]

$$k_D(|\mathbf{E}|) = k_D^0 F(w(|\mathbf{E}|)), \tag{5}$$

where F is the Onsager function and $w(|\mathbf{E}|)$ is the enhanced dissociation rate coefficient.

$$F(w(|\mathbf{E}|)) = \frac{I_1(4w(|\mathbf{E}|))}{2w(|\mathbf{E}|)}, \quad w(|\mathbf{E}|) = \frac{L_B}{L_O} = \left(\frac{e_0^3|\mathbf{E}|}{16\pi\varepsilon k_B^2 T^2}\right)^{1/2}. \tag{6}$$

Here, $I_1(x)$ is the modified Bessel function of the first kind and order 1. L_B and L_O are the Bjerrum and Onsager distances, respectively[29]

$$L_B = \frac{e_0^2}{8\pi\varepsilon k_B T}, \qquad L_O = \sqrt{\frac{e_0}{4\pi\varepsilon|\mathbf{E}|}}. \tag{7}$$

L_B is the distance where the electrostatic energy between two ions becomes of the same order as the thermal energy. Two ions can be considered to be bounded in an ionic pair when their separation is smaller than L_B, as in that situation the thermal motion is not able to overcome their electrical attraction. The length L_O is the distance from a point charge where the magnitude of the external electric field $\mathbf{E}$ becomes of the same order as the electric field produced by the charge in the

liquid. In the expressions above, $\varepsilon = \varepsilon_r \varepsilon_0$ is the absolute permittivity (ε_r and ε_0 being the dielectric constant of the liquid and the permittivity of the vacuum, respectively). In order for the external electric field to affect the equilibrium of an associated ionic pair it has to be $L_O \leq L_B$, that is, the external electric field has to be strong enough to affect the electric attraction between the ions in an associated pair. When $|\mathbf{E}| = 0$ we have $w(0) = 0$ and $F(0) = 1$, and no enhancement occurs. When there is enhancement, we will assume the dissociation-recombination equilibrium is not appreciably modified[30]. Then, the equilibrium concentration of the ionic species is

$$n_{eq} = n_{eq}^0 \sqrt{F(w(|\mathbf{E}|))}, \tag{8}$$

where n_{eq}^0 is the concentration of ionic species with no external electric field applied. The electrical conductivity is proportional to the concentration of ionic species at equilibrium. For a symmetric electrolyte it is

$$\sigma = 2e_0 K n_{\mathrm{eq}}, \tag{9}$$

K being the ionic mobility. Then, the conductivity depends on the electric field as

$$\sigma = \sigma_0 \sqrt{F(w(|\mathbf{E}|))}, \tag{10}$$

where σ_0 stands for the electrical conductivity without field enhanced dissociation. The dielectric liquids used in EHD conduction pumping have conductivities in the range 10^{-11} to $10^{-7}\,\mathrm{S/m}$.

B. Electric equations and boundary conditions

The electrical magnitudes are described by the Poisson equation for the electric potential Φ, and the electrostatic field definition. In the volume of the liquid we have

$$\nabla \cdot (\varepsilon \nabla \Phi) = -e_0 (n_+ - n_-), \qquad \mathbf{E} = -\nabla \Phi. \tag{11}$$

Here, n_+ and n_- are the volume concentration of positive and negative species, respectively.

With regard to the boundary conditions, the metallic electrodes will have a fixed electric potential. Special consideration must be given to the electric boundary conditions on the non-metallic substrates. Whenever an electrolyte is in contact with a surface, with no external electric field applied, an electrical double layer (EDL) develops[15,16]. The simplest EDL structure comprises one layer of ions rigidly adhered on the surface of the solid, the Stern layer, and a diffuse layer near the surface, the Debye layer. The length scale of this Debye layer is given by eq. (2). For a working temperature of 300 K and a typical value of the dielectric constant $\varepsilon_r = 5$, we get values of the Debye length varying between 1 and $30\,\mu\mathrm{m}$ for the liquids typically used in EHD conduction pumping. Hence, in macro and meso-sized pumps the effect of the EDL can be safely ignored. However, this is not the case if we consider systems with typical dimensions of tens of microns. The electric field created by the imposed electric potential is going to perturb the natural charge distribution in the EDL. And the EDL next to the substrate can affect the performance of the EHD conduction pump.

The ions in the Stern layer can be assumed to remain stuck on the interface, unless very high electric fields are applied ($10^9\,\mathrm{V/m}$)[15]. Then, the right boundary condition on the surface of the substrate is a uniform surface charge density, σ_S, representing the Stern layer, assumed to be constant. The magnitude of this surface charge can be estimated from measurements of the zeta potential, ζ, when the EDL is in its non disturbed state, that is, with no normal external electric field applied[16]. The ζ potential is the electrical potential difference between the surface and the electroneutral bulk of the liquid. Using the Debye-Hückel approximation, the electric potential of the non disturbed EDL can be approximated as

$$\Phi_{EDL} \simeq \zeta e^{-z/\lambda_D}, \tag{12}$$

where z is the distance to the interface. The volumetric charge density in the Debye layer is

$$\rho_{EDL} = -\nabla \cdot (\varepsilon \nabla \Phi_{EDL}) = -\frac{\varepsilon \zeta}{\lambda_D^2} e^{-z/\lambda_D}. \tag{13}$$

Now, we can estimate the total charge in the Debye layer

$$Q_{EDL} = S \int_0^\infty \rho_{EDL}(z)\,\mathrm{d}z = -\frac{\varepsilon \zeta S}{\lambda_D}. \tag{14}$$

Here S is the area of the interface. As the liquid is electroneutral, the total charge in the Stern layer is $-Q_{EDL}$, so the surface charge is

$$\sigma_S = \frac{\varepsilon \zeta}{\lambda_D}. \tag{15}$$

This expression corresponds to the surface charge on an infinite plane that would produce an electric field ζ/λ_D, that is, the order of magnitude of the electric field across the unperturbed Debye layer.

Let us stress that we use the value of the zeta potential only as a way to estimate the value of the intrinsic surface charge appearing on the interface between a liquid and a solid substrate. It is an experimental parameter characteristic of a given substrate-liquid pair. The value of the electric potential on the substrate during an EHD conduction experiment is not ζ in general. This would mean that the electric field would be normal to the interface, and this is not the case. Also, we do not use the Debye-Hückel approximation in our model for EHD conduction pumping. It is used here to estimate the value of σ_S from the value of ζ obtained from experiments where the Debye-Hückel approximation is valid.

Then, the electric boundary conditions for each type of surface are

$$\begin{aligned} &\text{positive electrode :} && \Phi = \Phi_0, \\ &\text{negative electrode :} && \Phi = 0, \\ &\text{substrate :} && \mathbf{n} \cdot \nabla \Phi = \sigma_S / \varepsilon. \end{aligned} \tag{16}$$

Here, $\mathbf{n}$ is the unit vector normal to the surface of the substrate pointing from the liquid towards the substrate.

The volume of the substrate has to be included in the model only if the polarization surface charge on the substrate is relevant. This polarization charge is produced by the different values of the dielectric constant in the liquid and the substrate. Its magnitude is related to the jump of the normal components of the electric field at both sides of the interface. If the external applied field is mainly parallel to the substrates, the effect of this polarization surface charge is already taken into account in the zeta potential. If this is not the case, the substrate volume must be included in the computational domain.

C. Transport equations and boundary conditions

As we have discussed in Section II A, in the liquids used in EHD conduction pumping the concentration of the neutral species, c_0, can be considered constant. The conservation equations for the concentration of the positive and negative species, n_+ and n_-, are

$$\frac{\partial n_\pm}{\partial t} + \nabla \cdot \mathbf{F}_\pm = k_D(|\mathbf{E}|)c_0 - k_R n_+ n_-. \tag{17}$$

The first therm on the right hand side corresponds to dissociation, while the second term represents recombination. The fluxes densities $\mathbf{F}_\pm$ are

$$\mathbf{F}_\pm = \pm n_\pm K_\pm \mathbf{E} + n_\pm \mathbf{u} - D_\pm \nabla n_\pm, \tag{18}$$

The first term represents the electric drift, the second one the advection by the fluid and the third one the diffusion. In this paper we will assume that the two ionic species have the same values for the ionic mobility and diffusion coefficients, thus $K_+ = K_- = K$ and $D_+ = D_- = D$. We will take for k_R the upper bound determined by Langevin, $k_R = 2e_0K/\varepsilon$[31]. With all these assumptions, and using (6), the transport equations read

$$\begin{aligned}\frac{\partial n_\pm}{\partial t} + \nabla \cdot (n_\pm(\mathbf{u} \pm K\mathbf{E}) - D\nabla n_\pm) = \\ = \frac{2e_0K(n_{\text{eq}}^0)^2}{\varepsilon}\left(F(w(|\mathbf{E}|) - \frac{n_+n_-}{(n_{\text{eq}}^0)^2}\right).\end{aligned} \tag{19}$$

We discuss now carefully the role of diffusion. In the electroneutral bulk and inside the heterocharge layers diffusion is negligible. In the bulk the ratio of the diffusive current and the electric drift is

$$\frac{D|\nabla n_\pm|}{n_\pm K|\mathbf{E}|} \approx \frac{D/d}{KE_0} = \frac{k_BT/e_0}{E_0 d} = \frac{\Phi_T}{\Phi_0}. \tag{20}$$

We have used the Einstein relation here, $D = Kk_BT/e_0$. The thermal potential is $\Phi_T = kBT/e_0 \approx 25\,\text{mV}$ at room temperature. The applied potential is always much higher than Φ_T, even for micro-sized systems. For example, for $d = 10\,\mu\text{m}$ and $E_0 = 10^6\,\text{V/m}$ it is $\Phi_0 = 10\,\text{V}$. This is the reason why diffusion is usually neglected in EHD bulk flows[32].

Inside the heterocharge layer the length scale is given by the heterocharge thickness, λ_H, given by (3). Then the ratio is

$$\frac{D|\nabla n_\pm|}{n_\pm K|\mathbf{E}|} \approx \frac{D/\lambda_H}{KE_0} = \frac{\sigma_0 k_B T}{e_0 K \varepsilon E_0^2} = 6\times10^{-3} - 6\times10^{-7} \ll 1. \tag{21}$$

We have taken $\sigma_0 = 10^{-11} - 10^{-7}\,\text{S/m}$, $K \approx 10^{-8}\,\text{m}^2/\text{V}\cdot\text{s}$, $\varepsilon_r \approx 5$, $T \approx 300\,\text{K}$, $E_0 = 10^6\,\text{V/m}$. These are typical values in EHD conduction pumping experiments. Hence, next to the metallic electrodes, inside the heterocharge layers, we can neglect diffusion.

However, the situation is different on non-metallic substrates. The applied electric field generated by the electrodes is typically parallel to the substrates. Then the EDL naturally present does not disappear completely, as it is the case near metallic electrodes. In macro-systems this EDL can be safely ignored[1]. However, we want to develop a model that can be applied to EHD pumps of all sizes. Then we have to keep the charge diffusion in the model, in order to describe the distribution of electric species next to the non-metallic substrates.

We discuss now the boundary conditions for the ionic species. On the positive metallic electrode, any positive ion created by dissociation near the electrode is pushed away by the Coulomb force. Therefore, we have $n_+ = 0$. As we retain the diffusive term, we need a boundary condition for the flux of the negative species on the positive electrode. The electric current through the positive electrode is sustained by the flux of negative species given by the electric drift term, diffusion being negligible as we have discussed above. Hence, we impose as boundary condition a normal zero gradient of the species concentration. This boundary condition implies that there is no accumulation of species next to the electrode. Once the ions get neutralized they move with the flow and reenter the dissociation-recombination process. This discussion is valid for the negative metallic electrode with the polarities reversed.

As for the non-metallic substrate, there is no transfer of charge between the ionic species and the substrate. Then, the flux of ionic species must be null on the substrate. Thus, the general boundary conditions for each of the typical physical boundaries are

$$\begin{aligned}&\text{positive electrode}: && n_+ = 0, && \mathbf{n}\cdot\nabla n_- = 0,\\ &\text{negative electrode}: && n_- = 0, && \mathbf{n}\cdot\nabla n_+ = 0,\\ &\text{substrate}: && \mathbf{F}_\pm\cdot\mathbf{n} = 0.\end{aligned} \tag{22}$$

D. Hydrodynamic equations and boundary conditions

The hydrodynamic equation are the momentum equation and the continuity equation

$$\begin{aligned}\rho_m\left(\frac{\partial \mathbf{u}}{\partial t} + \mathbf{u}\cdot\nabla\mathbf{u}\right) &= -\nabla P + \mu\nabla^2\mathbf{u} + \mathbf{F}_E,\\ \nabla\cdot\mathbf{u} &= 0.\end{aligned} \tag{23}$$

Here, $\mathbf{u}$ is the fluid velocity, P is the pressure, ρ_m is the fluid density and μ is the dynamic viscosity. The electric force $\mathbf{F}_E$

has three components: the Coulomb force, the dielectric force and the electrostriction force[29,33]

$$\mathbf{F}_E = q\mathbf{E} - \frac{1}{2}E^2\nabla\varepsilon + \nabla\left(\frac{1}{2}\rho_m\left(\frac{\partial\varepsilon}{\partial\rho_m}\right)_T E^2\right). \tag{24}$$

As we are assuming the liquid to be isothermal, the permittivity is uniform and the dielectric force does not appear. The electrostriccion force, being the gradient of a scalar magnitude, can be included in the pressure. Hence, only the Coulomb force has to be considered. The expression in terms of the species densities is:

$$\mathbf{F}_E = q\mathbf{E} = e_0(n_+ - n_-)\mathbf{E}. \tag{25}$$

The hydrodynamic boundary conditions are no-slip for the three types of physical surfaces.

E. Dimensionless governing equations, boundary conditions and parameters

In this section, the dimensionless physical magnitudes are expressed with an asterisk. We choose these scales for each physical magnitude

$$\begin{array}{llll} x,y\sim d, & n_\pm \sim n^0_{\rm eq}, & E\sim E_0, & \Phi\sim E_0 d,\\ u\sim KE_0, & t\sim d/KE_0, & P\sim \rho_m K^2 E_0^2. & \end{array} \tag{26}$$

Here, d is a typical length characterising the size of the system. This model is intended to be applied to EHD pumps sized from centimetres to tens of micrometers. We have chosen the order of magnitude of the imposed field, E_0 as the relevant electrical magnitude, and we derive the scale for the applied electric potential from it. The reason is that, in the experiments, we will be working at the maximum electric field without charge injection from the electrodes, in order to get a greater electric force. So it is E_0 who is going to characterize the regime. In EHD conduction pumps E_0 if of the order of several MV/m. The time scale is the transit ionic time.

With these scales the non-dimensional equations are

$$\frac{\partial n^*_\pm}{\partial t^*} + \nabla\cdot(n^*_\pm(\mathbf{u}^*\pm\mathbf{E}^*)) - \alpha\nabla^2 n^*_\pm = \\ = 2C_0(F(w(|\mathbf{E}^*|) - n^*_+ n^*_-), \tag{27}$$

$$\nabla^2\Phi^* = -C_0(n^*_+ - n^*_-), \tag{28}$$

$$\mathbf{E}^* = -\nabla\Phi^*, \tag{29}$$

$$\frac{\partial \mathbf{u}^*}{\partial t^*} + \mathbf{u}^*\cdot\nabla\mathbf{u}^* = -\nabla P^* + \tag{30}$$

$$+\frac{1}{Re^E}\nabla^2\mathbf{u}^* + M^2C_0(n^*_+ - n^*_-)\mathbf{E}^*, \tag{31}$$

$$\nabla\cdot\mathbf{u}^* = 0. \tag{32}$$

The non-dimensional parameters in these equations are

$$C_0 = \frac{e_0 n^0_{eq} d}{\varepsilon E_0},\ \ \alpha = \frac{k_B T}{e_0 E_0 d},\ \ Re^E = \frac{\rho_m K E_0 d}{\mu},\ \ M = \frac{\sqrt{\varepsilon/\rho_m}}{K}. \tag{33}$$

The number C_0 is the conduction number. Using (9) it can be written as

$$C_0 = \frac{\sigma_0 d}{2\varepsilon K E_0}. \tag{34}$$

This number is a key parameter to differentiate the two limit regimes in EHD conduction: ohmic and saturation. We discuss thoroughly these regimes in the next section. The number α is the diffusion number. It can be understood as the ratio of the thermal electric field generated by the thermal agitation, $E_T = k_B T/e_0 d$, and E_0. As we have discussed in Section II C, diffusion is always negligible in the electroneutral bulk and inside the heterocharge layers. However, we keep diffusion to be able to apply the model to micro-sized pumps where the effect of the natural surface charge on non-metallic substrates can be relevant. The number Re_E, the electric Reynolds number, is a Reynolds number built with the ionic velocity. Typical values in EHD conduction pumps range from 5000 for centimeter sized pumps to 5 for sizes of the order of $10\,\mu$m. Let us stress that this is not the hydrodynamic Reynolds number. The electric Reynolds number plays the role of a non-dimensional applied electric field. The mobility number M is the ratio of the so-called hydrodynamic mobility and the ionic mobility[34]. It only depends on the liquid properties. In the experiments, the value of M is typically lower than 10, although for very viscous liquids can be of order of 1000.

The Onsager function with the non dimensional electric field can be written as

$$F(w) = \frac{I_1(4w)}{2w}, \qquad w(|\mathbf{E}^*|) = O^{1/2}\,|\mathbf{E}^*|^{1/2}, \tag{35}$$

where the Onsager non-dimensional number O is

$$O = \frac{e_0^3 E_0}{16\pi\varepsilon k_B^2 T^2} \tag{36}$$

When $O \geq 1$ the enhanced dissociation by the electric field is relevant. Therefore, the typical value of the applied electric field where this happens is

$$O = 1 \Longrightarrow E_0 = \frac{16\pi\varepsilon k_B^2 T^2}{e_0^3} \simeq 9\,\mathrm{MV/m}. \tag{37}$$

This value has been computed with $\varepsilon_r = 5$ and room temperature. In the experiments the value of this number is in the range $O \in [0.1, 2]$.

However, for a given pump the value of O changes with the applied voltage. It would preferable to define a non-dimensional number that characterizes the behavior of a given pump. The relevant non-dimensional number related to E_0 here is the conduction number, C_0. We then define a new non-dimensional number as

$$O = \beta^2/C_0 \Longrightarrow \beta = \left(\frac{e_0^3\sigma_0 d}{32\pi\varepsilon^2 K k_B^2 T^2}\right)^{1/2}. \tag{38}$$

This number depends only on operational values of the EHD pump. In this way, the Onsager function can be computed as

$$F(w) = \frac{I_1(4w)}{2w}, \qquad w(|\mathbf{E}^*|) = \beta\, C_0^{-1/2} |\mathbf{E}^*|^{-1/2}. \tag{39}$$

We will see in Section III that β can be used to identify the regime the operating regime for a given EHD conduction pump. In experiments, β is small for micro-sized pumps and around 30 for pumps in the centimeter range.

The non-dimensional boundary conditions on each boundary type are

$$\begin{aligned}
&\text{pos. electrode}: && n_+^* = 0, && \mathbf{n}\cdot\nabla n_-^* = 0,\\
& && \Phi^* = 1, && \mathbf{u}^* = \mathbf{0},\\
&\text{neg. electrode}: && \mathbf{n}\cdot\nabla n_+^* = 0, && n_-^* = 0,\\
& && \Phi^* = 0 && \mathbf{u}^* = \mathbf{0},\\
&\text{substrate}: && \mathbf{n}\cdot\left(\pm n_\pm^* \mathbf{E}^* - \alpha \nabla n_\pm^*\right) = 0, &&\\
& && \mathbf{n}\cdot\nabla\Phi^* = \Lambda, && \mathbf{u}^* = \mathbf{0}.
\end{aligned} \tag{40}$$

The parameter Λ is a new dimensional number defined as

$$\Lambda = \frac{\zeta}{E_0 \lambda_D}. \tag{41}$$

The dimensionless surface charge density Λ describes the effect of the Stern surface charge. It can be written as $\Lambda = E_S/E_0$, where $E_S = \zeta/\lambda_D$ is the order of magnitude of the electric field created by the Stern layer. This parameter has an interesting physical interpretation for micro-sized pumps. When $\Lambda \ll 1$ it is $E_T \ll E_0$ and the external field dominates the charge distribution near the substrate. This is the regime where EHD conduction pumps work. When $\Lambda \gg 1$ the electric field generated in the EDL dominates. This is the situation for electroosmosis pumps. Then, Λ characterizes the transition from electoosmodis pumping to EHD conduction pumping.

Equations (27)-(32) along with definition (35) and boundary conditions (40) define the mathematical model for EHD conduction pumping. These equations can only be solved numerically, even for the simplest configurations.

F. Comparison with experimental data

In order to validate the model, we compare the outcome of our simulations with the results from experiments described in Pearson and Seyed-Yagoobi [10]. In that work, the authors use as liquid the refrigerant R-123. In the provided specifications, the values of the physical magnitudes are $\varepsilon_r = 4.9$, $\mu = 4.3\times10^{-4}\,\mathrm{Pa\cdot s}$, $\rho_m = 1.47\times10^3\,\mathrm{kg/m^3}$. We estimate the ionic mobility from the Walden's rule[35], and it is $K \simeq 5\times10^{-8}\,\mathrm{m^2/V\cdot s}$. The conductivity can vary in the range $10^{-7} - 10^{-8}\,\mathrm{S/m}$. All the simulations presented in this section have been made with $\sigma_0 = 10^{-7}\,\mathrm{S/m}$ and the other properties values provided above. The typical size of the micro-pump described in the paper is $d = 50\,\mu\mathrm{m}$. The temperature for the simulations is $T = 293\,\mathrm{K}$. These computations do not pretend to obtain accurately the experimental values of electric current and generated pressure, as there are physical properties not well known, notably the ionic mobilities of the species. Our aim is to obtain the correct orders of magnitude and overall trends of the physical quantities. The numerical simulations have been performed with COMSOL Multiphysics uses the finite element method. The Navier-Stokes equations are solved with streamline and crosswind stabilization[36,37]. The transport equations are solved using the Transport of Diluted Species module with the scheme from Gomes Dutra Do Carmo and Galeão [38]. The computations were performed on progressive refined meshes until the maximum variation in the results were smaller than 5%.

Figure 2 depicts the geometric configuration used in the computation. The configuration is two dimensional. It has been constructed with the same relative dimensions as the experimental pump described in Pearson and Seyed-Yagoobi [10]. The location of the metallic electrodes and the substrate is indicated. We impose periodic boundary conditions at the left and right borders and symmetry boundary condition at the top border. The color plot corresponds to the non-dimensional charge density computed as $q_t = n_+ - n_-$. The heterocharge layers next to each electrode are clearly visible. The streamlines of the fluid velocity are also plotted. The computation was done with $E_0 = 12\,\mathrm{MV/m}$ and zeta potential $\zeta = 25\,\mathrm{mV}$.

Figure 3 plots the results from numerical simulations along with experimental data. The first plot shows the values of the electric current. We see that the numerical simulation gives the right order of magnitude of the measured current. The second plot shows the maximum generated pressure measured when there is no net flow in the circuit. We see that the fit is acceptable. To obtain the values of ΔP_{max} in the numerical simulation, we apply an adverse pressure gradient Δp at the right border, increasing the value of Δp until the net flow is zero. In order to apply this pressure drop COMSOL fix the pressure to be zero at a point on the left border of the domain, while imposing at the right border a normal stress corresponding to the given value of the pressure drop. An alternative way of achieving this is to impose a uniform force on the domain, along the X direction, of absolute value $\Delta p/L_x$, L_x being the horizontal length of the domain. We have performed some computations using these technique to check that we get the same results with both methods. Once the value of ΔP_{max} has been computed for a pair of electrodes, we multiply this

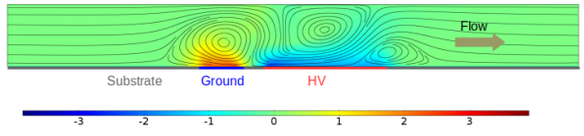

FIG. 2. Geometric configuration for the numerical simulations of Section II F. The color plot shows the non-dimensional net electric charge. The streamlines of the flow are also plotted. The geometry is two dimensional.

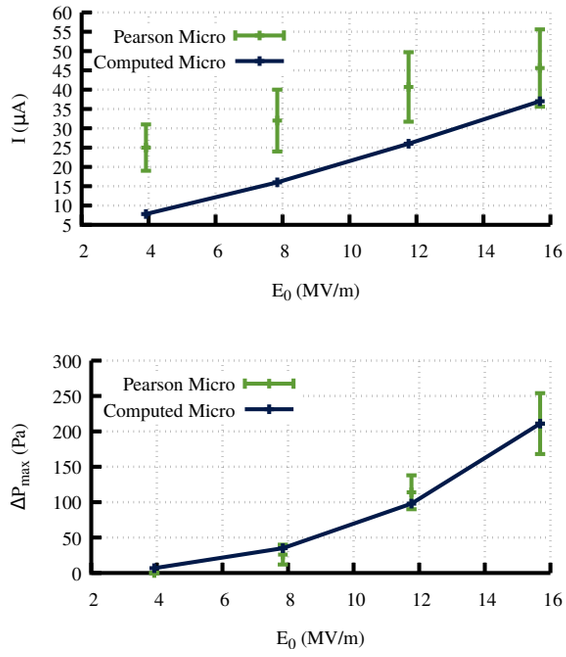

FIG. 3. Comparison of experimental values from the micro-pump in Pearson and Seyed-Yagoobi [10] with computed ones. The first plot shows the electric current and the second plot shows the maximum generated pressure without net flow.

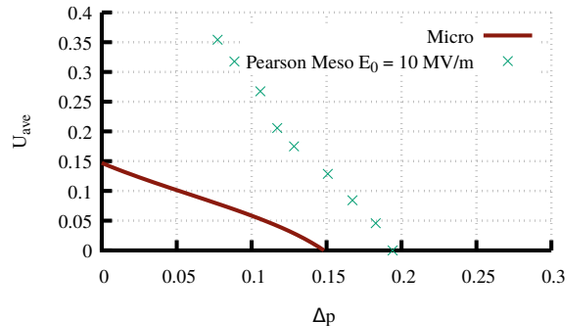

FIG. 4. Evolution of the non-dimensional average velocity with the adverse pressure gradient for the computed values for the micro-pump compared with data from the meso-pump from Pearson and Seyed-Yagoobi [10]. The behavior is similar, although the slope is different.

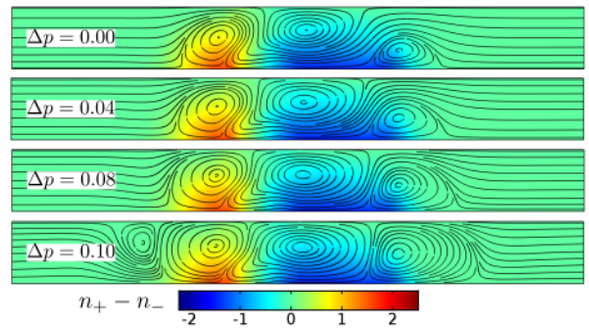

FIG. 5. Streamlines of the flow and net non-dimensional charge for several values of the adverse pressure gradient imposed. The bottom case corresponds to an average flow velocity almost null.

number by 10, accounting for the 10 non-interacting pairs of electrodes in the experiment. In this way, we reproduce the pressure drop produced by the hydraulic circuit outside the pump. Figure 4 plots the evolution of the computed dimensionless average velocity versus the adverse pressure gradient. The evolution is quasi linear, indicating that the structure of the flow changes very little as the value of the adverse pressure gradient is increased. In order to confirm this, Figure 5 shows the streamlines of the flow, along with the net non-dimensional net electric charge, for different values of the adverse pressure gradient Δp. The global structure of the flow changes very little as the value of Δp is increased. Only the plot at the bottom, for $\Delta p = 0.10$, shows a new roll at the left of the domain. For this value the average net velocity is almost zero. This correspond to the region of closer to horizontal axis in the line in Figure 4, where the evolution diverges more from linearity.

We have also included in Figure 4 one series of experimental data of the maximum generated pressure vs applied potential from the meso-pump in Pearson and Seyed-Yagoobi [10]. They do not provide these data for the micro-pump. Anyway, we have included the data from their biggest pump to show that the trend is similar to what we obtain with our numerical simulations for the micro-pump. The slope is different, due to the different sizes of the pumps.

III. CONDUCTION REGIMES

Here we analyze in detail the characteristics of the EHD conduction mechanisms in the two limiting regimes: ohmic and saturation. These regimes have been discussed elsewhere[1,14,30]. We show that the new parameter β, along with the conduction number C_0, are the relevant parameters to characterize the regime that EHD conduction pumps operate in, including the enhanced dissociation by the electric field. Here, we are particularly interested in the dependence of the generated pressure with C_0 and β. This has not been discussed in the aforementioned works. In this section, all the equations are dimensionless. We drop the asterisks for the sake of clarity.

Let's consider a simple 2D planar geometry with two parallel electrodes a distance d apart as depicted on Figure 6. An electric voltage V_0 is applied between the electrodes, so that the typical electric field is $E_0 = V_0/d$. There is no motion of the liquid, as the electrodes are symmetric and the ionic mobilities of the species are assumed to be identical. We can also neglect diffusion, as there is no substrate. We look for sta-

tionary solutions. Also, the physical magnitudes depend only on the coordinate x, hence, the mathematical problem is 1D. Then, equations (27)-(32) reduce to

$$\pm\frac{\mathrm{d}(n_\pm E)}{\mathrm{d}x} = 2C_0(F(w(|E|)) - n_+n_-), \tag{42}$$

$$\frac{\mathrm{d}^2\Phi}{\mathrm{d}x^2} = -C_0\,(n_+ - n_-), \tag{43}$$

$$E = -\frac{\mathrm{d}\Phi}{\mathrm{d}x}. \tag{44}$$

The Onsager function $F(w)$ is defined in (35). The boundary conditions are

$$n_+(0) = 0, \quad n_-(1) = 0, \quad \Phi(0) = 1, \quad \Phi(1) = 0. \tag{45}$$

The numerical results presented in this section have been computed numerically using a 1D model of the problem described by equations (42)-(44) and boundary conditions (45). The computations have been made with COMSOL Multiphysics.

A. Regime characterization

The number C_0, from the expression (34), can be written as the ratio of two typical times: the ionic transit time $\tau_K = d/KE_0$, which is the typical time needed by the ions to travel from one electrode to the other, and the ohmic time $\tau_\sigma^0 = \varepsilon/\sigma_0$ which is the typical time the ions take to recombine, in absence of the Onsager-Wien effect. Hence $C_0 = \tau_K/2\tau_\sigma^0$. The distance an ion created by dissociation near one of the electrodes typically travels before recombining is

$$\lambda_H \simeq KE_0\tau_\sigma^0 = \frac{1}{2C_0}d. \tag{46}$$

When $C_0 \gg 1$ we have $\tau_\sigma^0 \ll \tau_K$ and $\lambda_H \ll d$, this is the ohmic regime. In this case, the heterocharge layers are very thin and the bulk is electroneutral. The first plot in Figure 7 shows the distribution of positive and negative species along with the electric field. These profiles have been computed with $C_0 = 10$ and $\beta = 0$, that is, without Onsager-Wien effect. The heterocharge layers and the electroneutral bulk are well delimited. The color plot in Figure 6 represents the distribution of net electric charge for the same configuration, computed as $(n_+ - n_-)$.

When $C_0 \ll 1$, it is $\tau_K \ll \tau_\sigma^0$ and $\lambda_H \gg d$. This means that the heterocharge layers overlap, and there is no electroneutral bulk. The ions typically leave the liquid before they have time to recombine. This is the saturation regime. The second plot in figure 7 plots the distribution of positive and negative species along with the electric field for $C_0 = 0.1$ and $\beta = 0$. We can see that the concentrations of species are very low, as the ions leave the domain before they have time to recombine. As a consequence the value of the net electric charge is small, and the non-dimensional electric field is very close to 1 in the whole domain.

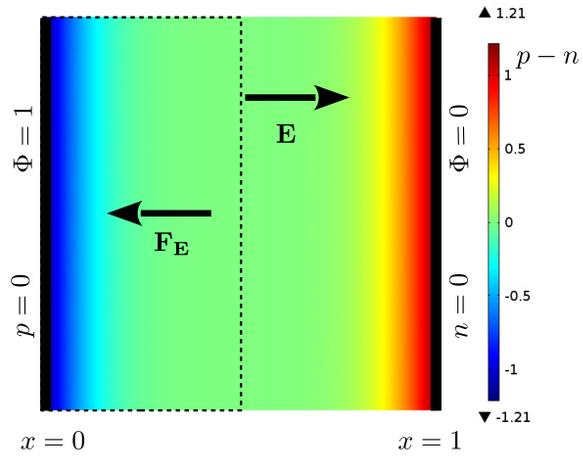

FIG. 6. Dimensionless configuration for the 2D parallel plates case, along with the net electric charge distribution in the ohmic regime, with no flow motion. The heterocharge layers at each electrode are clearly visible. The computation has been made for $C_0 = 10$, with no Onsager-Wien effect.

In fact, when electric field enhanced dissociation is considered, we have to replace the ohmic time above by $\tau_\sigma = \varepsilon/\sigma = \tau_\sigma^0/\sqrt{F(w)}$, where we have used (10). That is, the conduction regimes are better described by the combination[30]

$$C_0^E = C_0\sqrt{F(w_0)}, \qquad w_0 = \beta C_0^{-1/2} = \sqrt{O}. \tag{47}$$

Here, w_0 is given by (35) when the magnitude of the non-dimensional electric field $\mathbf{E}$ is 1. We will use $F_0 = F(w_0)$. If $C_0^E \gg 1$ we are in the ohmic regime. If $C_0^E \ll 1$ we are in the saturation regime.

B. Ohmic regime

The ohmic regime, where $C_0^E \gg 1$, is characterized by the existence of two heterocharge layers next to the electrodes and an electroneutral bulk. As it is discussed in Atten and Seyed-Yagoobi [1], we can use a boundary layer approximation. The analysis made by these authors is an extension to liquids of the boundary layer analysis applied in gas phase by Thomson and Thomson [39]. We will work only with the left half of the domain, as the distribution of species and electric field are symmetric. Then, we have an heterocharge layer for $0 < x < \lambda$ and an electroneutral bulk for $\lambda < x < 1/2$. Here, $\lambda = \lambda_H/d$. The heterocharge layers appear because ions produced near the electrodes of opposite polarity typically travel a distance λ before they recombine. The ions of the opposite polarity to the electrode have few counter-ions around them to recombine. Then, inside the heterocharge layers recombination can be neglected. Mathematically, the recombination terms n_+n_- in the equations (42) are negligible compared to the dissociation term because of the boundary conditions $p = 0$ and $n = 0$ at the electrodes. The Onsager function is not constant inside the heterocharge layer, but we simplify the problem assuming that $F(w(|E|)) \simeq F(w(|E(x=0)|)) = F_e$, that is, it takes the

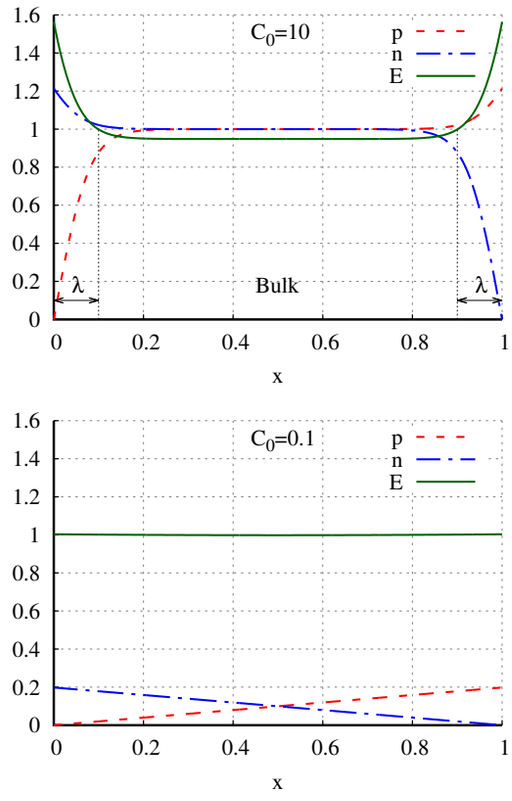

FIG. 7. Non-dimensional values of the concentration of positive and negative species and the electric field, without Onsager-Wien effect. For $C_0 = 10$ (top), in the ohmic regime, the heterocharge layers and the electroneutral bulk are clearly delimited. For $C_0 = 0.1$ (bottom), in the saturation regime, there is no electroneutral bulk. Also, the non-dimensional electric field in the saturation regime is very close to 1.

value at the electrode[30]. We also neglect diffusion, as we are inside the heterocharge layer (see Section II C). With these assumptions, equations (42)-(44) inside the heterocharge layer, corresponding to the positive electrode, $0 < x < \lambda$, reduce to

$$\pm\frac{\mathrm{d}(n_\pm E)}{\mathrm{d}x} = 2C_0F_e, \tag{48}$$

$$\frac{\mathrm{d}E}{\mathrm{d}x} = C_0(n_+ - n_-). \tag{49}$$

$$\tag{50}$$

with boundary conditions

$$n_+(0) = 0, \quad n_-(\lambda) = \sqrt{F_b}, \quad E(\lambda) = E_b. \tag{51}$$

Here, E_b is the electric field in the bulk and $F_b = F(E_b)$. The second equation expresses that, in the electroneutral bulk, the dissociation-ionization process is in equilibrium. Then the values of the concentrations of ionic species are the equilibrium ones, given by (8). These equations are easily solved to

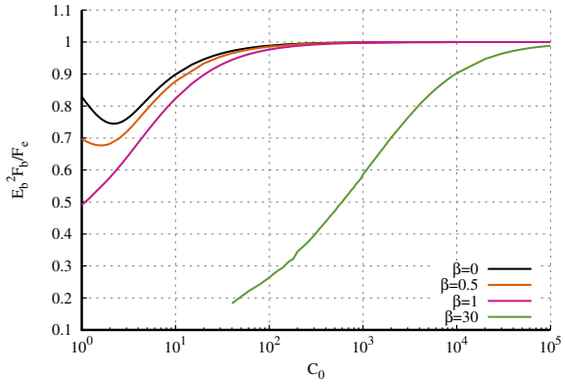

FIG. 8. Factor $E_b^2F_b/F_e$ vs. C_0 for different values of β.

get

$0 < x < \lambda$:

$$E(x) = \sqrt{4C_0^2F_ex^2 - 4C_0\sqrt{F_b}E_bx + \left(1+\frac{F_b}{F_e}\right)E_b^2},$$

$$n_+(x) = \frac{2C_0F_ex}{E(x)},$$

$$n_-(x) = \frac{2\sqrt{F_b}E_b - 2C_0F_ex}{E(x)}. \tag{52}$$

$\lambda < x < 1/2$:

$$E(x) = E_b,$$

$$n_\pm(x) = \sqrt{F_b}.$$

The width of the heterocharge layer is

$$\lambda = \frac{E_b}{2C_0}\frac{\sqrt{F_b}}{F_e}. \tag{53}$$

In this symmetric configuration there is no net electric force on the liquid. However, we can explore the dependence of the generated pressure computing the electric force on the left half of the fluid domain, delimited by the dotted rectangle in Figure 6. We have

$$\Delta P_e = \int_0^{1/2}(n_+ - n_-)E\,\mathrm{d}x = \int_0^{\lambda}(n_+ - n_-)E\,\mathrm{d}x = -\frac{E_b^2}{2C_0}\frac{F_b}{F_e}. \tag{54}$$

We have used (52) to compute the integral. The negative sign implies that the force is directed towards the left electrode. From now on, ΔP_e will mean the absolute value of the generated pressure.

In experimental conditions, β has a wide range of values. For pumps of centimeter size it can be $\beta \simeq 30$. Figure 8

plots the evolution of the factor $E_b^2 F_b/F_e$ vs. C_0. These plots have been obtained integrating numerically equations (42)-(44) along with boundary conditions (45). When $C_0 \gg 1$ this factor becomes independent of C_0 and equal to 1. Therefore, in this limit the dimensionless generated pressure scales as

$$\Delta P_e \simeq \frac{1}{2C_0}. \tag{55}$$

This asymptotic law will be more accurate for small and moderate values of β. Actually, it is exact if there is no enhanced dissociation. However, in the experiments, high values of β implies high values of C_0. For example, if $\beta = 30$, typically C_0 ranges from 700 to 12000. From Figure 8 it can be seen that for these values of C_0 the factor depends only weakly on C_0.

In this limit the dimensionless current density is

$$J = n_-(0)E(0) \simeq 2. \tag{56}$$

The reference scale for the current density is $J_0 = \sigma E_0/2$.

The dependence of the corresponding dimensional magnitudes on the applied electric field is

$$\Delta P_e^{\rm dim} \propto E_0^2 \propto V_0^2, \qquad \Delta J^{\rm dim} \propto E_0 \propto V_0. \tag{57}$$

C. Saturation regime

In this regime, we have $C_0^E \ll 1$. From equation (46), the heterocharge layers span all the volume between electrodes, overlapping, as it can be seen in the second plot in Figure 7. Hence, there is no electroneutral bulk. Also, the ions typically leave the liquid before they have time to recombine. Then, we can again neglect recombination, but now in the entire volume. For C_0^E to be very small, it is necessary that $C_0 \ll 1$, because the value of the Onsager function is not small in this limit. Then, the source term in the Poisson equation (28) is very small and the non-dimensional electric field is very close to 1, the value corresponding to no net charge in the volume. The electric field can be expanded in powers of the small parameter C_0[30]

$$E(x) \simeq 1 + 2C_0^2 F_0 \left(x^2 - x + \frac{1}{6}\right). \tag{58}$$

For completeness, this expression is derived in Appendix A.

In the limit $C_0 \ll 1$, equations (42)-(44) become

$$\pm \frac{{\rm d}n_\pm}{{\rm d}x} = 2C_0 F_0. \tag{59}$$

with boundary conditions

$$n_+(0) = 0, \qquad n_-(1) = 0. \tag{60}$$

Solving these equations we find

$$n_+(x) = 2C_0 F_0 x, \qquad n_-(x) = 2C_0 F_0 (1-x). \tag{61}$$

These are linear functions on x spanning all the volume between electrodes.

From and (58) and (61), the generated pressure is

$$\Delta P_e = \left| \int_0^{1/2} (n_+ - n_-) E \, {\rm d}x \right| \simeq \frac{1}{2} C_0 F_0. \tag{62}$$

In the limit $C_0 \ll 1$, the argument of the Onsager function, w_0, is large. The Bessel function can be substituted by the Hankel asymptotic expansion[40]. Thus, the value of F_0 in this limit is

$$F_0 \simeq \frac{1}{4\sqrt{2\pi}\beta^{3/2}} C_0^{3/4} e^{4\beta C_0^{-1/2}}. \tag{63}$$

The generated pressure using this asymptotic expression is

$$\Delta P_e^a \simeq \frac{C_0^{7/4} e^{4\beta C_0^{-1/2}}}{8\sqrt{2\pi}\beta^{3/2}}. \tag{64}$$

For the electric current density we have

$$J \simeq n_-(0)E(0) = 2C_0 F_0, \tag{65}$$

and the asymptotic expression is

$$J^a \simeq \frac{C_0^{7/4} e^{4\beta C_0^{-1/2}}}{2\sqrt{2\pi}\beta^{3/2}}. \tag{66}$$

If no Onsager-Wien effect is included, we get

$$\Delta P_e^a \simeq -\frac{1}{2} C_0, \qquad J^a \simeq 2C_0. \tag{67}$$

In this case, the corresponding dimensional magnitudes, $\Delta P_e^{\rm dim}$ and $J^{\rm dim}$ are independent of E_0, that is, of the applied potential.

D. Discussion on the conduction regimes

The first plot in Figure 9 shows the behavior of the computed dimensional electric current, $I \propto J/C_0$, with the dimensional average electric field, $E_0 \propto C_0^{-1}$. The values in these plots have been obtained solving numerically equations (42)-(44), along with boundary conditions (45). The line $\beta = 0$ corresponds to the case where the Onsager-Wien effect has been discarded. In this situation the regimes are fully characterized by the value of C_0. The ohmic regime, $C_0^{-1} \ll 1$, corresponds to low values of the electric field. Here, the electric current is proportional to the electric field. In the saturation regime, $C_0^{-1} \gg 1$, the dimensional electric current reaches a saturation value, independent of the applied electric field.

When the enhanced dissociation is considered, we have $\beta > 0$. For small values of β the effect of the enhanced dissociation is to increase the current in the saturation regime. As β increases, the saturation regime disappears. The current increases always with the electric field. For all values of β the current becomes proportional to the electric field for small enough values of E_0. This behavior can be explained observing the second plot in Figure 9. There, we plot the value of

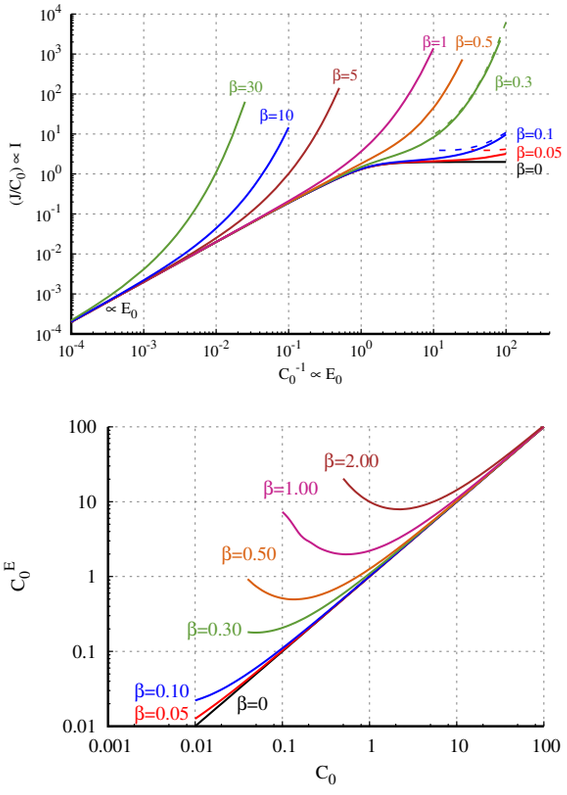

FIG. 9. The first plot shows the behavior of the dimensional current vs. the dimensional average electric field, for different values of β. The dashed lines correspond to the asymptotic expression (66). The second plot shows the value of C_0^E vs. C_0. In both cases, $\beta = 0$ corresponds to non enhanced dissociation. Although the magnitudes represented in both axes are non-dimensional, they have been chosen to be proportional to the dimensional current and the dimensional electric field.

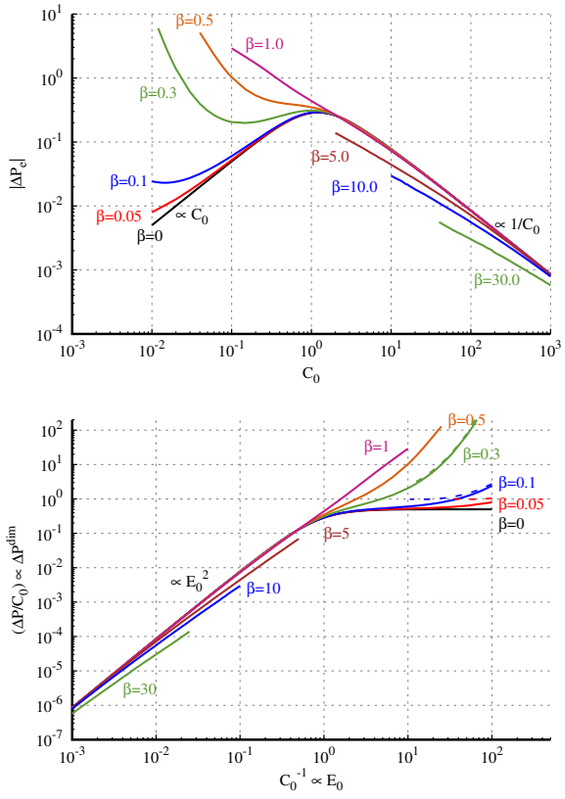

FIG. 10. The first plot shows the generated pressure vs. C_0 for different values of β. The dashed lines correspond to the asymptotic expression (66). The line $\beta = 0$ corresponds to non-enhanced dissociation. The second plot shows the behavior of the dimensional generated pressure vs. E_0. Although the magnitudes represented in both axes are dimensionless, they have been chosen to be proportional to the dimensional generated pressure and the dimensional electric field.

$C_0^E = C_0\sqrt{F_0}$ as a function of C_0 for different values of β. For high values of β, it is always $C_0^E > 2$. Then, saturation regime is never attained. This means that the structure of heterocharge layers and electroneutral bulk depicted in the first plot of Figure 7 exists even for high values of the electric field, that is, for C_0 small. The enhanced dissociation is able to create enough ions in the volume to compensate the ions leaving the domain.

For small values of β, when decreasing C_0 (which means increasing E_0) the system goes from the ohmic to the saturation regime. The dashed lines in the second plot correspond to the approximation given in the saturation regime by (66) for each value of β. The asymptotic expression for F_0 in (63) is valid up to a 5% of the real value when

$$\beta C_0^{-1/2} = O^{1/2} > 2 \Longrightarrow C_0 < \beta^2/4. \tag{68}$$

Then, as β increases, the maximum value of C_0 for which the asymptotic expression is accurate increases. Although, for the sake of clarity, it is not showed in the plot, if the integral in (62) is used to compute the generated pressure the match is excellent for all values of β while in the saturation regime.

The first plot in Figure 10 shows the absolute value of the generated pressure as a function of C_0. For the case $\beta = 0$ the generated pressure is proportional to C_0 in the saturation regime ($C_0 \ll 1$) and to C_0^{-1} in the ohmic regime ($C_0 \gg 1$). When the Onsager-Wien effect is included, and in the ohmic regime, the generated pressure is proportional to C_0^{-1} for small and moderate values of β. The reason is that in the approximate expression (54), the factor $E_b^2 F_0/F_e$ is very close to one for all values of β. For higher values of β we observe a deviation, although if the value of C_0 is high enough the same dependency is recovered. Similarly to what is observed in the current, for $\beta > 1$ there is no saturation regime. The generated pressure keeps increasing when the applied field E_0 is increased. The second plot shows how the dimensional pressure depends on the applied electric field for the same values of β.

When β is small, a saturation regime is observed for small values of C_0. Here, the approximated expression (67) is valid only for very small values of β, and for C_0 not much smaller

than 1. The dashed lines correspond the asymptotic values given by (64). As it was the case with the electric current, the maximum value of C_0 for this expression to be accurate increases with β. Again, although it is not included in the plot, if the approximate value given by (62) is used to compute the generated pressure the match is excellent, while we stay in the saturation regime.

This analysis shows that the working regime of an EHD conduction pump, including enhanced dissociation by the electric field, can be characterized by two non-dimensional parameters: β and C_0. For a given system, β only depends on the physical properties of the liquid, the size of the system and the temperature, not on the applied electric potential. For $\beta \gtrsim 1$, the system remains always in the ohmic regime, and the generated pressure is proportional to C_0^{-1} for high enough values of E_0. We can explain this in terms of the structure of the heterocharge layers. The ohmic regime is characterised by the existence of two heterocharge layers separated by a electroneutral bulk. When the applied field increases (decreasing C_0), the heterocharge layers tend to become thicker and overlap. The ions have time to recombine before leaving the liquid. However, the Onsager-Wien increases the number of ions. For $\beta \geq 1$ the enhanced dissociation produces enough ions to preserve the structure of non-overlapping heterocharge layers with an electroneutral bulk. For small β (small systems and/or very non-conducting liquids) the enhanced dissociation cannot preserve this structure, the heterocharge layers overlap and a saturation regime arises, although somewhat affected by the enhanced dissociation.

It must be pointed out that, for a given system, with fixed β, not all the values of C_0 plotted in figure 10 can be reached experimentally. In typical conditions, the applied electric field cannot be greater than $15\,\mathrm{MV/m}$, approximately. For greater values injection of electric charge at the electrodes occurs, and the model has to be modified in order to account for charge injection.

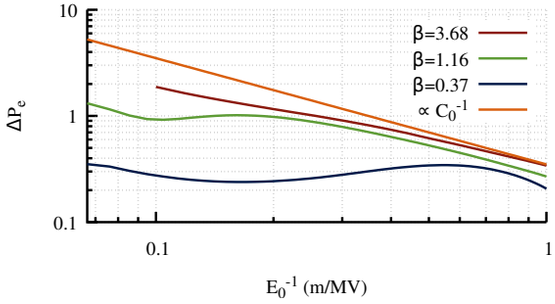

FIG. 11. Dimensionless maximum generated pressure vs. applied electric field computed with fluid motion. The trend line for the ohmic regime is included.

E. Influence of the motion of the fluid

The discussions in the previous sections did not include the fluid motion. Furthermore, real EHD conduction pumps have a more complicated geometry. We have performed some simulations computing the whole flow to explore the applicability of the regime discussion when the the motion of the fluid is included and a more realistic geometry is considered. We have used a computational domain similar to the one discussed in Section II F with $d = 50\,\mu\mathrm{m}$. We have computed the maximum generated pressure for three liquids with electrical conductivities $\sigma = 10^{-6}, 10^{-7}, 10^{-8}\,\mathrm{S/m}$. The first value is quite high, but it was chosen to get a high value of the parameter β for this given value of d. The dynamic viscosity of the liquid was $\mu = 2\times10^{-3}\,\mathrm{Pa\cdot s}$. We choose a high value of the viscosity in order to assure a small value of the Reynolds number, As we have discussed in Section II F, in this way the structure of the flow changes very little when an increasing adverse pressure gradient is imposed. The ionic mobility was computed from the Walden rule to be $K = 5\times10^{-9}\,\mathrm{m^2/V\cdot s}$. The simulations were done with an applied electric field E_0 ranging from 1 to 15 MV/m. These values correspond to the micro-pump experiment discussed in Pearson and Seyed-Yagoobi [10]. This figure has to be compared with the first plot in Figure 10. We can see that the trends are similar. In particular, for high values of β in the ohmic regime we get $\Delta P^e \propto C_0^{-1}$ with a good approximation. For $\beta = 3.68$ the system never enters the saturation regime. For $\beta = 1.16$ there is a slight saturation, but the Onsager-Wien effects quickly compensates the charge depletion. The curve for $\beta = 0.37$ is quite similar to the line for $\beta = 0.3$ in Figure 10. The pump enters the saturation regime quickly, and only for higher values of the applied electric field the Onsager-Wien effect is able to change the trend.

These simulations have been performed for a small pump, where the velocity of the liquid is not very high. For larger pumps the velocity of the liquid can overcome the electric drift velocity of the ions and perturb significantly the heterocharge layers. Anyway, in this case, both β and C_0 are very high. The pumps will always operate in an approximate ohmic regime with a clearly define electroneutral region between each electrode pair. In that case the dependence of the generate pressure with respect to C_0 predicted in Section III B should still be valid.

IV. CONCLUSIONS

In this paper, we have examined EHD conduction pumping in liquids with low conductivity. We have built a model of EHD conduction pumping that can be applied to pumps of all sizes, down to some tens of microns. The model assumes a weakly dissociated symmetric electrolyte, with two species with the same ionic mobility and diffusivity. The enhanced electric field dissociation, the Onsager-Wien effect, is also included. At the electrodes, the electrical boundary conditions are given by the imposed voltage. On the non-conductive surfaces, the electrical boundary condition consists of a fixed sur-

face charge, representing the Stern layer of the electrical double layer. The value of this surface charge can be estimated from experimental measurements of the ζ potential when the external applied electric field has no normal component to the substrate. The value of ζ is characteristic of a given combination substrate-liquid. The inclusion of this surface charge in our model introduces a new non-dimensional number, Λ, the ratio between the magnitudes of the natural electric field in the electrical double layer and the external applied field.

There are two typical regimes in EHD conduction pumping: the ohmic regime and the saturation regime. When electric enhanced dissociation is taken into account, the number $C_0^E = C_0\sqrt{F(w_0)}$, determines which one dominates, C_0 being the conduction number, $w_0 = \beta C_0^{-1/2}$ and $F(w_0)$ the Onsager function for w_0. These regimes have already been discussed in previous works. However, here we have highlighted how the generated pressure behaves in each regime. Two dimensionless numbers, β and C_0, characterize this behavior. The number β depends on liquid physical properties, the size of the system and the temperature. The number C_0 includes the influence of the applied electric field. When $\beta \gtrapprox 1$, the system is always in the ohmic regime even for high values of E_0 (low values of C_0). In this case, the Onsager-Wien effect is able to replenish the ions extracted from the liquid when the applied electric field is very high. Therefore, there are always two heterocharge layers and an electroneutral bulk. In this regime the non-dimensional generated pressure is proportional to C_0^{-1} for all values of β for a high enough value of E_0. Then, the dimensional generated pressure is proportional to E_0^2. For small values of β, the Onsager-Wien effect is not able to preserve the electroneutral bulk, and, when the applied electric field is increased, the system enters into the saturation regime. In that case, the dimensionless generated pressure is approximately proportional to C_0. The dimensional pressure would become independent of the applied electric field, but the enhanced dissociation introduces a small deviation. For intermediate values of β there is no saturation, although the increasing of the generated pressure with the applied electric field is slower than in the ohmic regime. Although the regime analysis has been performed without fluid motion, we have performed several computations to verify the predictions of the analysis when the motion of the fluid is considered.

ACKNOWLEDGMENTS

This work was funded with financial support from the Spanish Ministerio de Ciencia, Innovación y Universidades under Research Project No. PGC2018-099217-B-I00 (to P.A. Vázquez), the NASA Headquarters Micro-Gravity Fluid Physics Program (to M. Talmor and J. Seyed-Yagoobi) and the ANR program Edyphice as a part of the French national centre for scientific research (CNRS) (to P. Traoré). The work of M. Talmor was sponsored by a NASA Space Technology Research Fellowship. The authors would also like to thank Dr. L. Yang for his contribution to the experimental study.

Appendix A

We show here how to obtain the expression (58) for the electric field in the saturation regime. We provide a simplified version of the derivation described in Castellanos and Pontiga [30]. In this regime it is $C_0 \ll 1$. The ions leave the liquid before they have time to recombine. Therefore, we can neglect recombination in eqs. (42)-(44). Also, the electric field must be close to 1, as the source term in the Poisson equation is very small. Then, we can take $F(w(E)) \approx F_0$. With these approximations these equations can be written

$$\frac{\mathrm{d}(n_+E)}{\mathrm{d}x} = 2C_0F_0, \tag{A1}$$

$$\frac{\mathrm{d}(n_-E)}{\mathrm{d}x} = -2C_0F_0, \tag{A2}$$

$$\frac{\mathrm{d}E}{\mathrm{d}x} = C_0\,(n_+ - n_-). \tag{A3}$$

Subtracting (A2) from (A1) and introducing (A3) we get

$$\frac{\mathrm{d}E^2}{\mathrm{d}x} = A + 8C_0^2F_0x. \tag{A4}$$

Here, A is a constant. In order to get boundary conditions for this equation we multiply (A3) by E. Then, using (60) we get

$$\left.\frac{\mathrm{d}E^2}{\mathrm{d}x}\right|_{x=0} = -2C_0n_-(0)E(0) = -2C_0J, \tag{A5}$$

$$\left.\frac{\mathrm{d}E^2}{\mathrm{d}x}\right|_{x=1} = 2C_0n_+(1)E(1) = 2C_0J. \tag{A6}$$

Here, $J = n_-(0)E(0) = n_+(1)E(1)$ is the stationary current density. From (A4), (A5) and (A6) we obtain

$$J = 2C_0F_0, \qquad A = -4C_0^2F_0. \tag{A7}$$

Introducing the value of A in (A4) and integrating we obtain the electric field

$$E(x) = \sqrt{B + 4C_0^2F_0(x^2 - x)}. \tag{A8}$$

The constant B is obtained imposing that the non-dimensional potential drop between the electrodes is 1. Expanding $E(x)$ in powers of $C_0 \ll 1$ we get

$$\int_0^1 E(x)\,\mathrm{d}x = \sqrt{B} - \frac{F_0C_0^2}{3\sqrt{B}} = 1. \tag{A9}$$

Solving for B up to order C_0^2 it is

$$B = 1 + \frac{2}{3}F_0C_0^2. \tag{A10}$$

Introducing this expression in (A8) and expanding again in powers of $C_0 \ll 1$ we obtain (58).

[1]P. Atten and J. Seyed-Yagoobi, "Electrohydrodynamically induced dielectric liquid flow through pure conduction in point/plane geometry," IEEE Transactions on Dielectrics and Electrical Insulation **10**, 27–36 (2003).
[2]R. Gharraei, E. Esmaeilzadeh, and M. R. Heirani Nobari, "Numerical investigation of conduction pumping of dielectric liquid film using flush-mounted electrodes," Theoretical and Computational Fluid Dynamics **28**, 89–106 (2014).
[3]V. A. Chirkov, Y. Stishkov, and S. A. Vasilkov, "Characteristics of electrohydrodynamic pump of the dissociation type: low and high voltage ranges," IEEE Transactions on Dielectrics and Electrical Insulation **22**, 2709–2717 (2015).
[4]A. Sobhani, S. Nasirivatan, R. Gharraei, and E. Esmaeilzadeh, "Experimental investigation of fully developed falling film flow in the presence of conduction pumps," Journal of Electrostatics **73**, 71–79 (2015).
[5]R. Gharraei, M. Hemayatkhah, S. Baheri Islami, and E. Esmaeilzadeh, "An experimental investigation on the developing wavy falling film in the presence of electrohydrodynamic conduction phenomenon," Experimental Thermal and Fluid Science **60**, 35 – 44 (2015).
[6]M. Mirzaei and M. Saffar-Avval, "Enhancement of convection heat transfer using EHD conduction method," Experimental Thermal and Fluid Science **93**, 108–118 (2018).
[7]S.-I. Jeong and J. Seyed-Yagoobi, "Innovative electrode designs for electrohydrodynamic conduction pumping," IEEE Transactions on Industry Applications **40**, 900–904 (2004).
[8]M. A. W. Siddiqui and J. Seyed-Yagoobi, "Experimental study of pumping of liquid film with electric conduction phenomenon," IEEE Transactions on Industry Applications **45**, 3–9 (2009).
[9]M. Yazdani and J. S. Yagoobi, "Heat transfer enhancement of backstep flow by means of EHD conduction pumping," International Journal of Heat and Mass Transfer **73**, 819–825 (2014).
[10]M. R. Pearson and J. Seyed-Yagoobi, "Experimental study of EHD conduction pumping at the meso- and micro-scale," Journal of Electrostatics **69**, 479–485 (2011).
[11]V. K. Patel and J. Seyed-Yagoobi, "A Mesoscale Electrohydrodynamic-Driven Two-Phase Flow Heat Transport Device in Circular Geometry and In-Tube Boiling Heat Transfer Coefficient Under Low Mass Flux," Journal of Heat Transfer **137**, 41504 (2015).
[12]M. R. Pearson and J. Seyed-Yagoobi, "EHD conduction-driven enhancement of critical heat flux in pool boiling," IEEE Transactions on Industry Applications **49**, 1808–1816 (2013).
[13]S. A. Vasilkov, V. A. Chirkov, and Y. K. Stishkov, "Electrohydrodynamic flow caused by field-enhanced dissociation solely," Physics of Fluids **29**, 063601 (2017).
[14]A. Ramos, ed., *Electrokinetics and Electrohydrodynamics in Microsystems* (Springer, 2011).
[15]J. O. Bockris, A. K. N. Reddy, and M. E. Gamboa-Aldeco, *Modern electrochemistry. Volume 2A, Fundamentals of electrodics*, 2nd ed. (Kluwer, 2002).
[16]B. J. Kirby, *Micro- and Nanoscale Fluid Mechanics* (Cambridge University Press, 2010).
[17]J. R. Melcher, *Continuum Electromechanics* (MIT Press, 1981).
[18]M. Yazdani and J. Seyed-Yagoobi, "Effect of Charge Mobility on Electric Conduction Driven Dielectric Liquid Flow," in *2009 Electrostatics Joint Conference* (Boston, MA, USA, 2009) pp. 1–6.
[19]S.-I. Jeong, J. Seyed-Yagoobi, and P. Atten, "Theoretical/numerical study of electrohydrodynamic pumping through conduction phenomenon," IEEE Transactions on Industry Applications **39**, 355–361 (2003).
[20]M. Yazdani and J. Seyed-Yagoobi, "Electrically Induced Dielectric Liquid Film Flow Based on Electric Conduction Phenomenon," Dielectrics and Electrical Insulation, IEEE Transactions on **16**, 768–777 (2009).
[21]M. Yazdani and J. Seyed-Yagoobi, "Heat Transfer Augmentation of Parallel Flows by Means of Electric Conduction Phenomenon in Macro- and Microscales," Journal of Heat Transfer **132**, 62402 (2010).
[22]S. R. Mahmoudi, K. Adamiak, and G. S. P. Castle, "Prediction of the static pressure generation for an electrohydrodynamic conduction pump," Proceedings - IEEE International Conference on Dielectric Liquids (2011), 10.1109/ICDL.2011.6015459.
[23]Y. Feng and J. Seyed-Yagoobi, "Understanding of electrohydrodynamic conduction pumping phenomenon," Physics of Fluids **16**, 2432–2441 (2004).
[24]S. R. Mahmoudi, K. Adamiak, G. S. Peter Castle, and M. Ashjaee, "Study of electrohydrodynamic micropumping through conduction phenomenon," IEEE Transactions on Industry Applications **47**, 2224–2234 (2011).
[25]R. Gharraei, E. Esmaeilzadeh, M. Hemayatkhah, and J. Danaeefar, "Experimental investigation of electrohydrodynamic conduction pumping of various liquids film using flush electrodes," Journal of Electrostatics **69**, 43–53 (2011).
[26]H. Abe, Y. Imai, N. Tokunaga, Y. Yamashita, and Y. Sasaki, "Highly Efficient Electrohydrodynamic Pumping: Molecular Isomer Effect of Dielectric Liquids, and Surface States of Electrodes," ACS Applied Materials and Interfaces **7**, 24492–24500 (2015).
[27]V. K. Patel and J. Seyed-Yagoobi, "Combined Dielectrophoretic and Electrohydrodynamic Conduction Pumping for Enhancement of Liquid Film Flow Boiling," Journal of Heat Transfer **139**, 61502–61509 (2017).
[28]L. Onsager, "Deviations from Ohm's Law in Weak Electrolytes," Journal of Chemical Physics **2**, 599–615 (1934).
[29]A. Castellanos, ed., *Electohydrodynamics* (Springer-Verlag, 1998).
[30]A. Castellanos and F. Pontiga, "Generalised Thomson-Onsager model for charge injection into dielectric liquids," Proceedings of 1995 Conference on Electrical Insulation and Dielectric Phenomena , 616–620 (1995).
[31]P. Langevin, "Recherches sur les Gaz Ionisés," Annales de chimie et de physique **28**, 223 (1903).
[32]A. Castellanos, "Coulomb-driven Convection in Electrohydrodynamics," IEEE Transactions on Electrical Insulation **26**, 1201–1215 (1991).
[33]L. M. Landau and E. M. Lifshitz, *Electrodynamics of Continuous Media* (Addison-Wesley, 1971).
[34]N. J. Felici, "Phénomenes hydro et aérodynamiques dans la conduction des diélectriques fluides," Revue General d'Electrostatique **78**, 717–734 (1969).
[35]J. Lyklema, *Fundamentals of Interface and Colloid Science: Solid-Liquid Interfaces* (Academic Press, 1991).
[36]T. J. R. Hughes and M. Mallet, "A new finite element formulation for computational fluid dynamics: III. The generalized streamline operator for multidimensional advective-diffusive systems," Computer Methods in Applied Mechanics and Engineering **58**, 305–328 (1986).
[37]G. Hauke and T. J. R. Hughes, "A unified approach to compressible and incompressible flows," Computer Methods in Applied Mechanics and Engineering **113**, 389–395 (1994).
[38]E. Gomes Dutra Do Carmo and A. C. Galeão, "Feedback Petrov-Galerkin methods for convection-dominated problems," Computer Methods in Applied Mechanics and Engineering **88**, 1–16 (1991).
[39]J. J. Thomson and G. P. Thomson, *Conduction of electricity through gases*, 3rd ed. (Cambridge University Press, 1928).
[40]M. Abramowitz and I. Stegun, *Handbook of Mathematical Functions* (NIST, 1964).

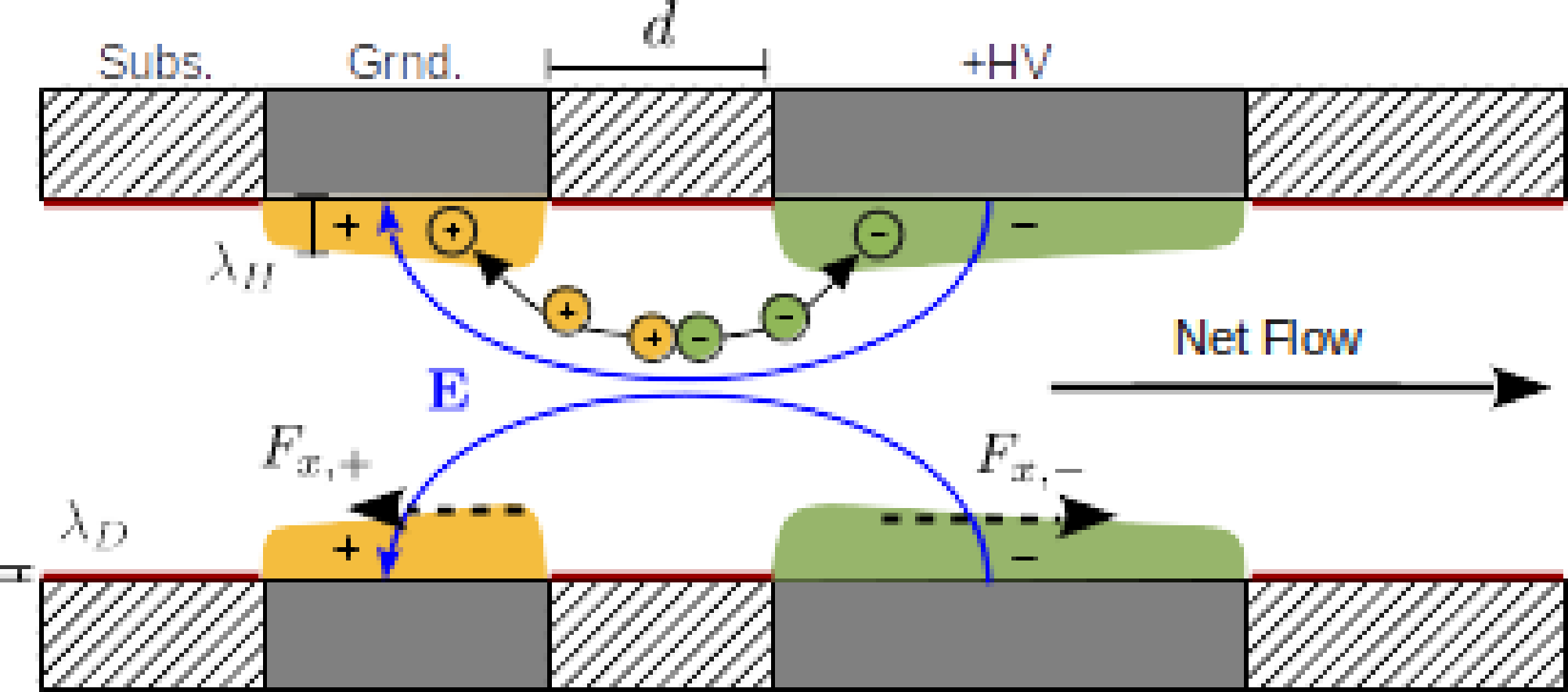
Subs.
Grnd.
d
+HV
λ_U
E
Net Flow
$F_{x,+}$
$F_{x,-}$
λ_D

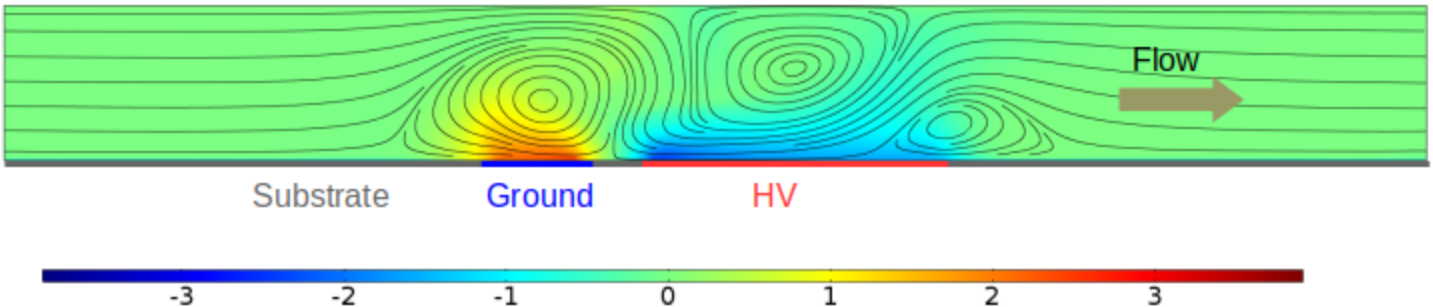
Flow
Substrate
Ground
HV
-3
-2
-1
0
1
2
3

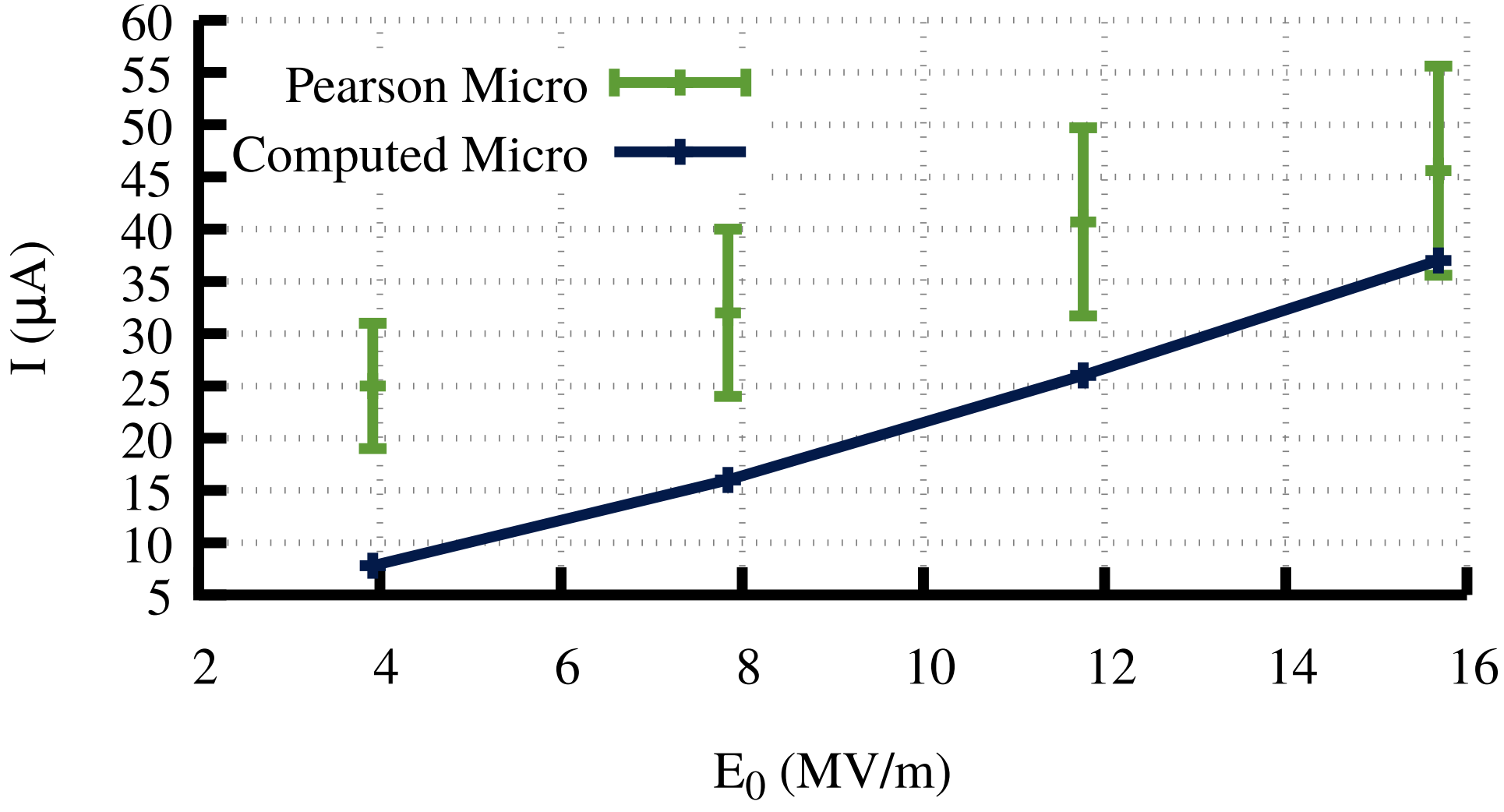
Pearson Micro
Computed Micro
I (μA)
60
55
50
45
40
35
30
25
20
15
10
5
2
4
6
8
10
12
14
16
E0 (MV/m)

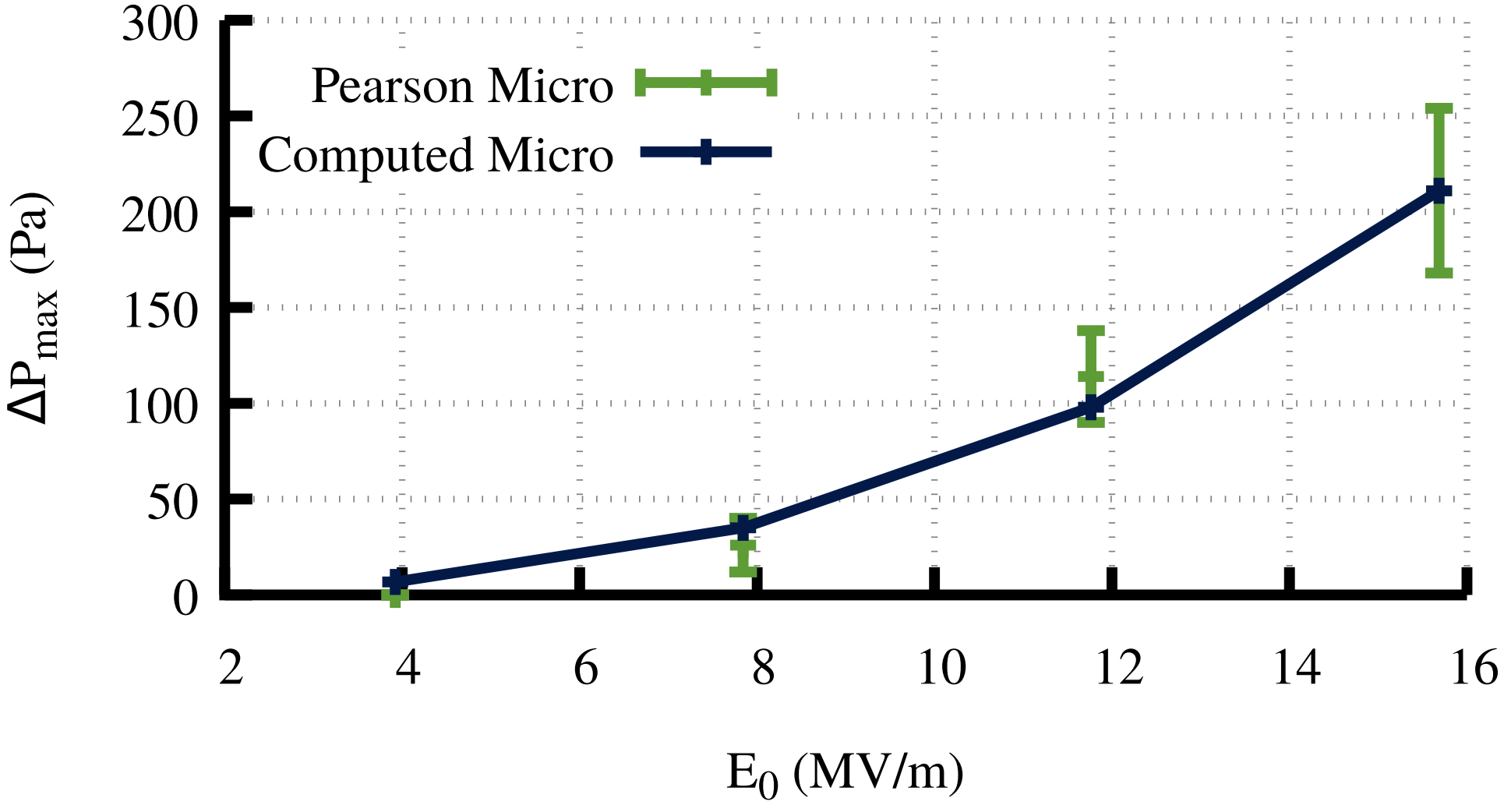
Pearson Micro
Computed Micro
300
250
200
150
100
50
0
ΔP_{max} (Pa)
2
4
6
8
10
12
14
16
E_0 (MV/m)

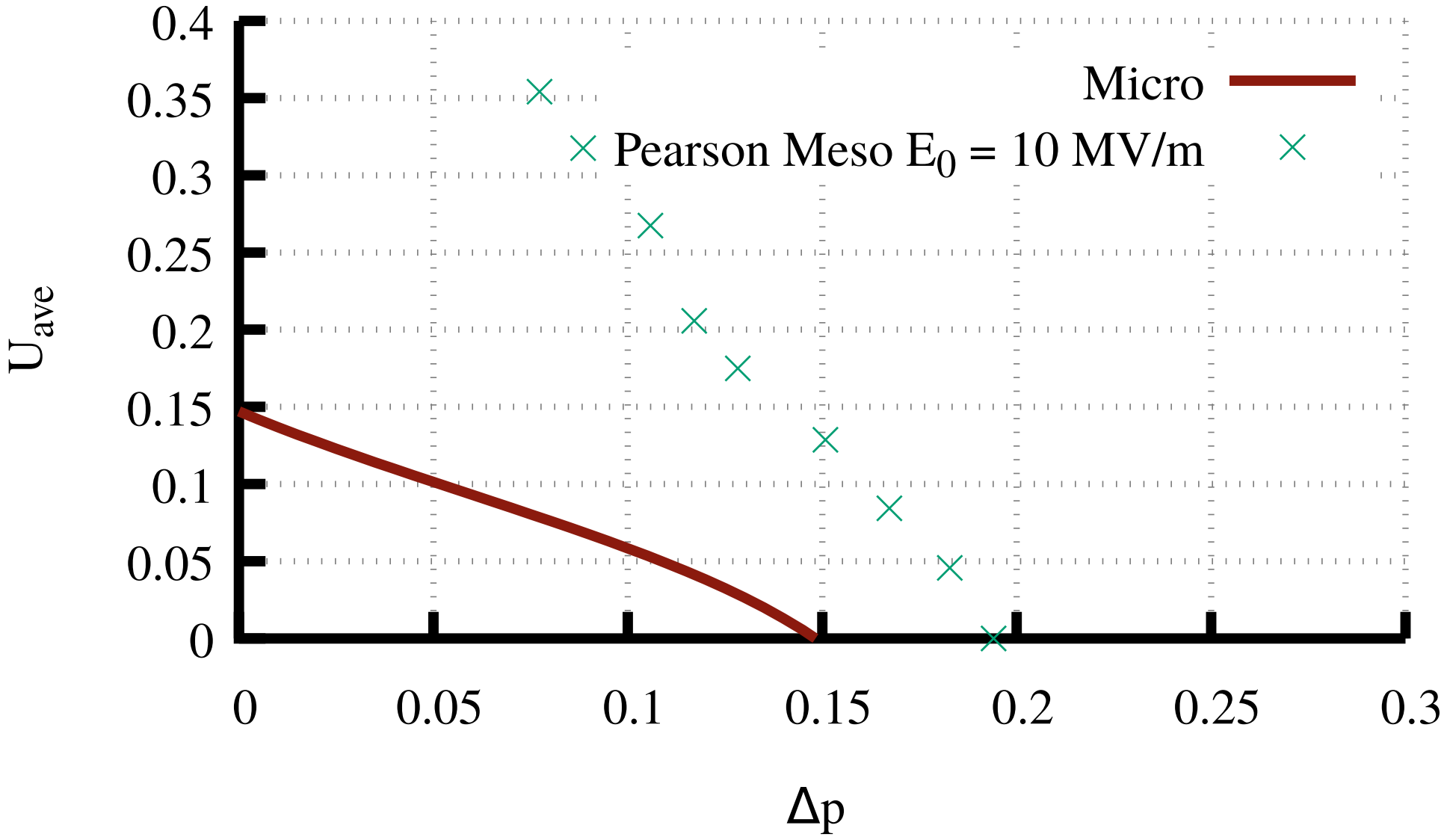
0.4
0.35
0.3
0.25
0.2
0.15
0.1
0.05
0
U_{ave}
0
0.05
0.1
0.15
0.2
0.25
0.3
Δp
Micro
Pearson Meso E_0 = 10 MV/m

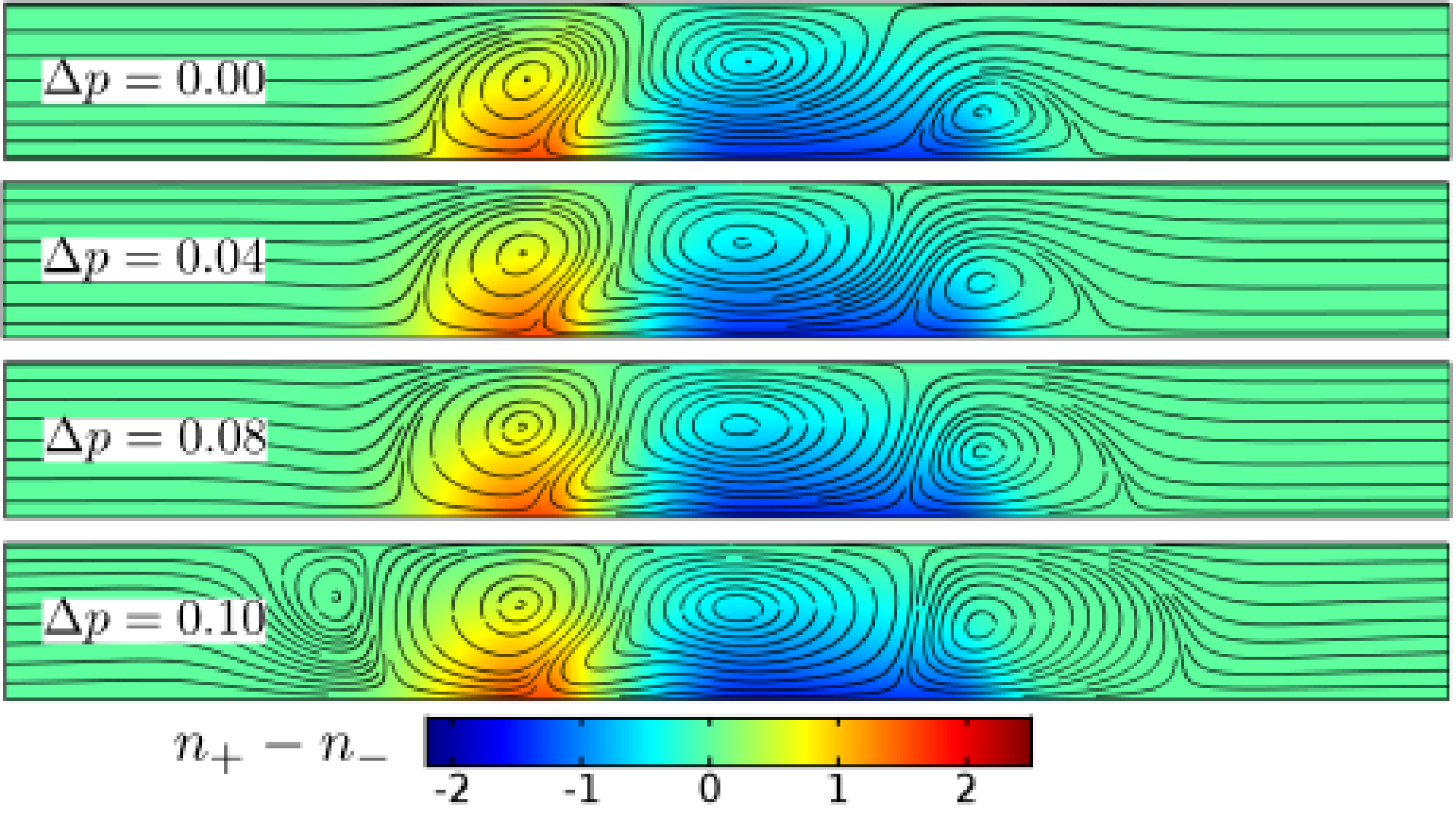
$\Delta p = 0.00$
$\Delta p = 0.04$
$\Delta p = 0.08$
$\Delta p = 0.10$
$n_+ - n_-$
-2
-1
0
1
2

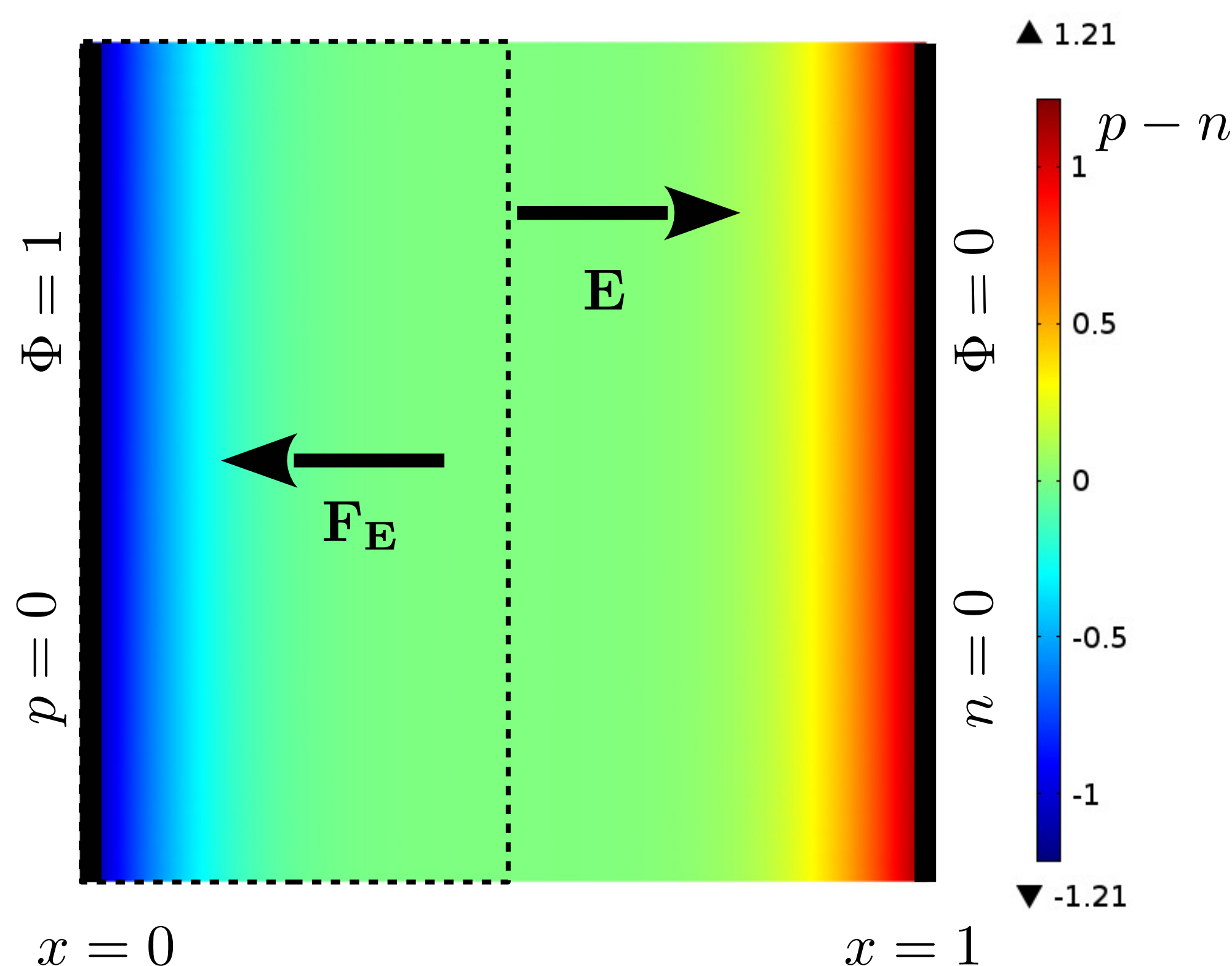
▲ 1.21
$p - n$
1
0.5
0
-0.5
-1
▼ -1.21
$\Phi = 1$
$\Phi = 0$
$p = 0$
$n = 0$
$\mathbf{E}$
$\mathbf{F_E}$
$x = 0$
$x = 1$

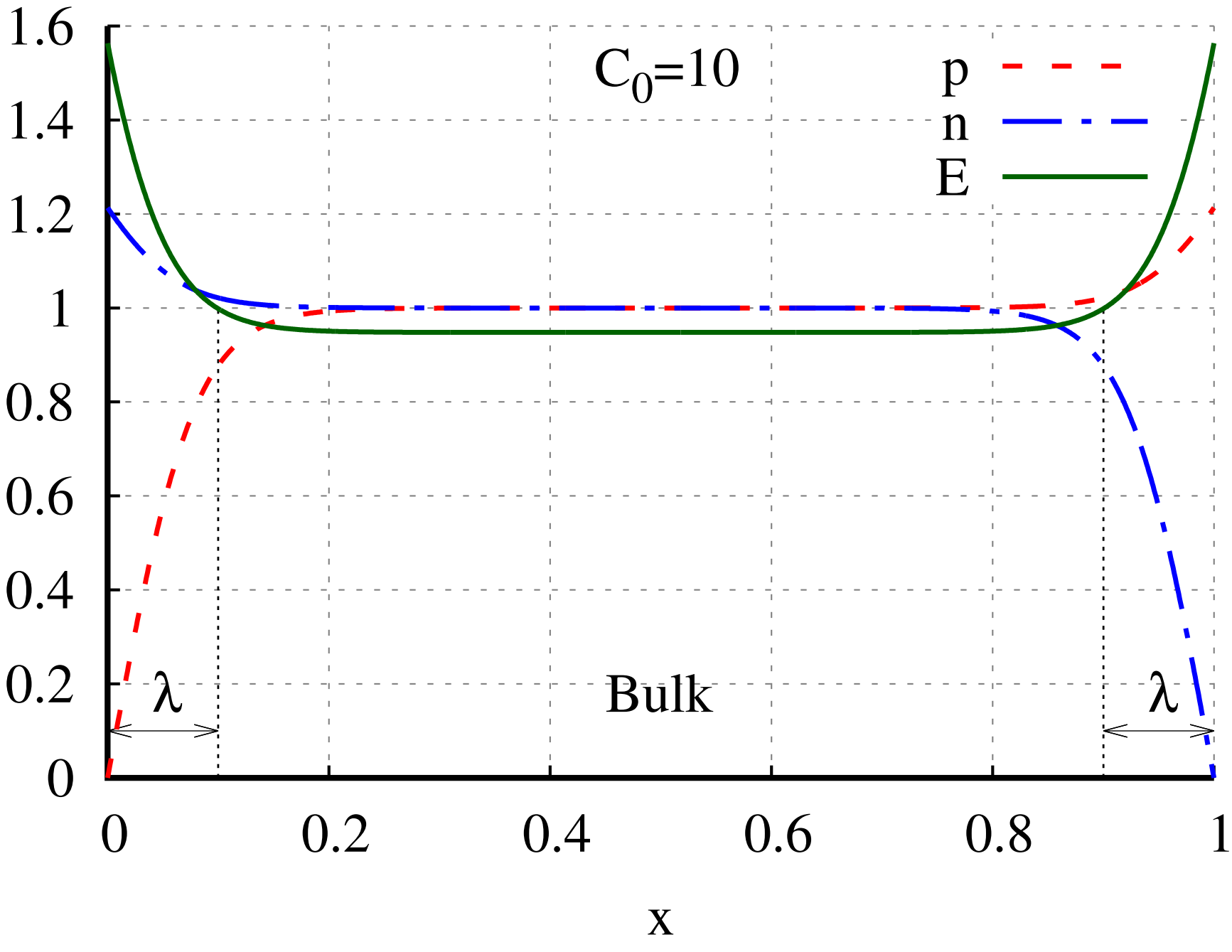
1.6
1.4
1.2
1
0.8
0.6
0.4
0.2
0
0
0.2
0.4
0.6
0.8
1
x
C0=10
p
n
E
λ
Bulk
λ

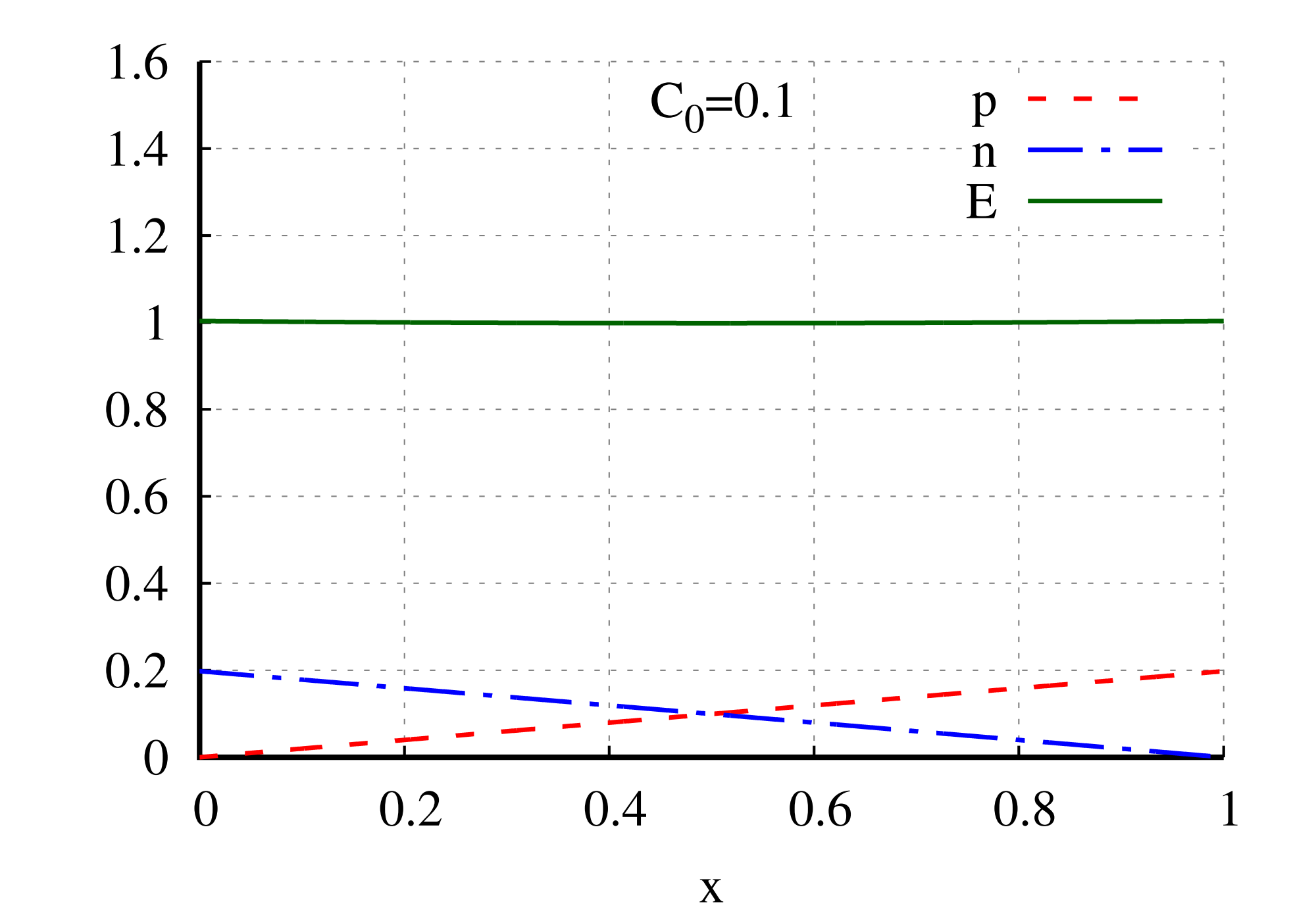
1.6
1.4
1.2
1
0.8
0.6
0.4
0.2
0
0
0.2
0.4
0.6
0.8
1
x
C0=0.1
p
n
E

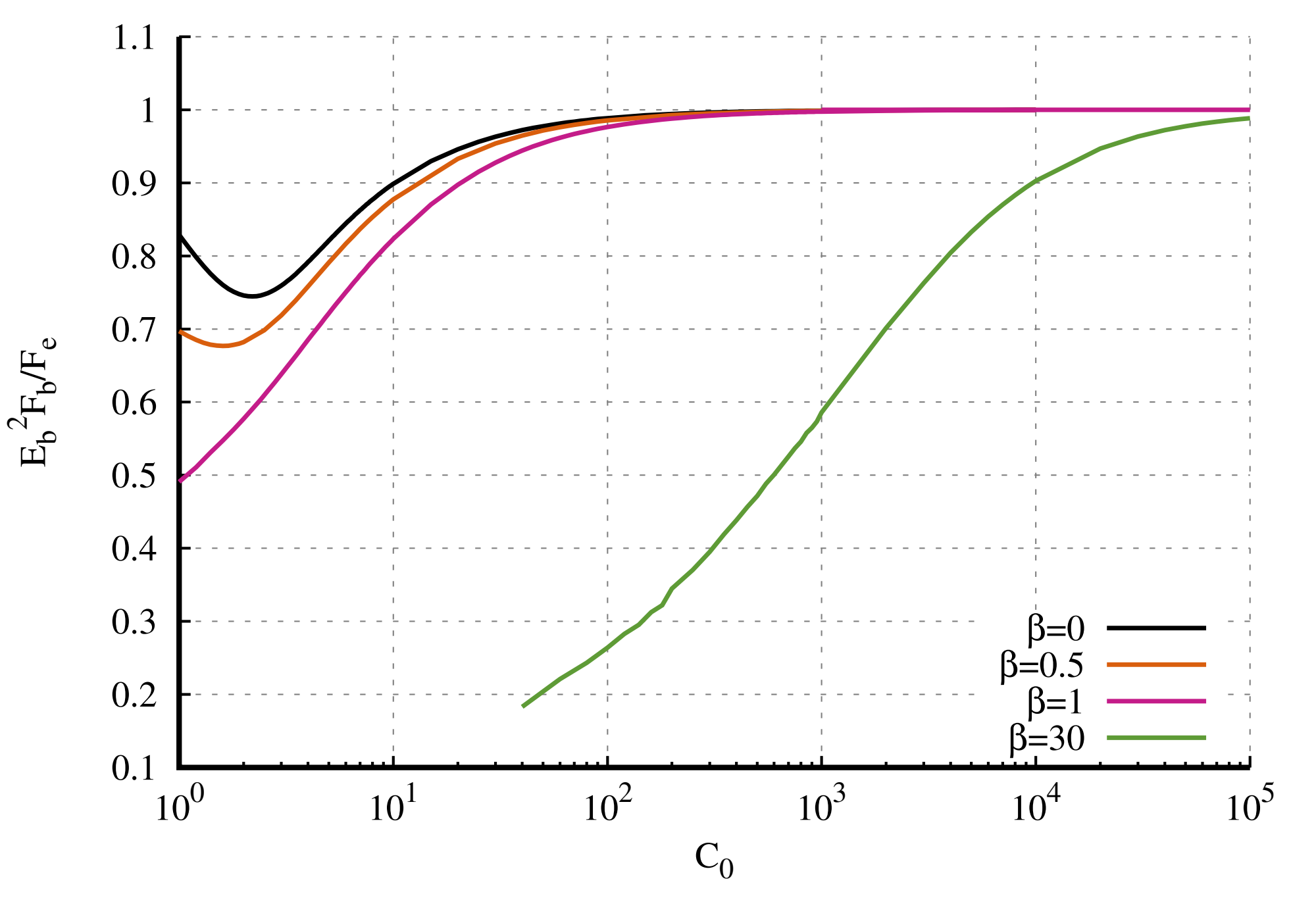
1.1
1
0.9
0.8
0.7
0.6
0.5
0.4
0.3
0.2
0.1
$E_b^2 F_b/F_e$
10^0
10^1
10^2
10^3
10^4
10^5
C_0
β=0
β=0.5
β=1
β=30

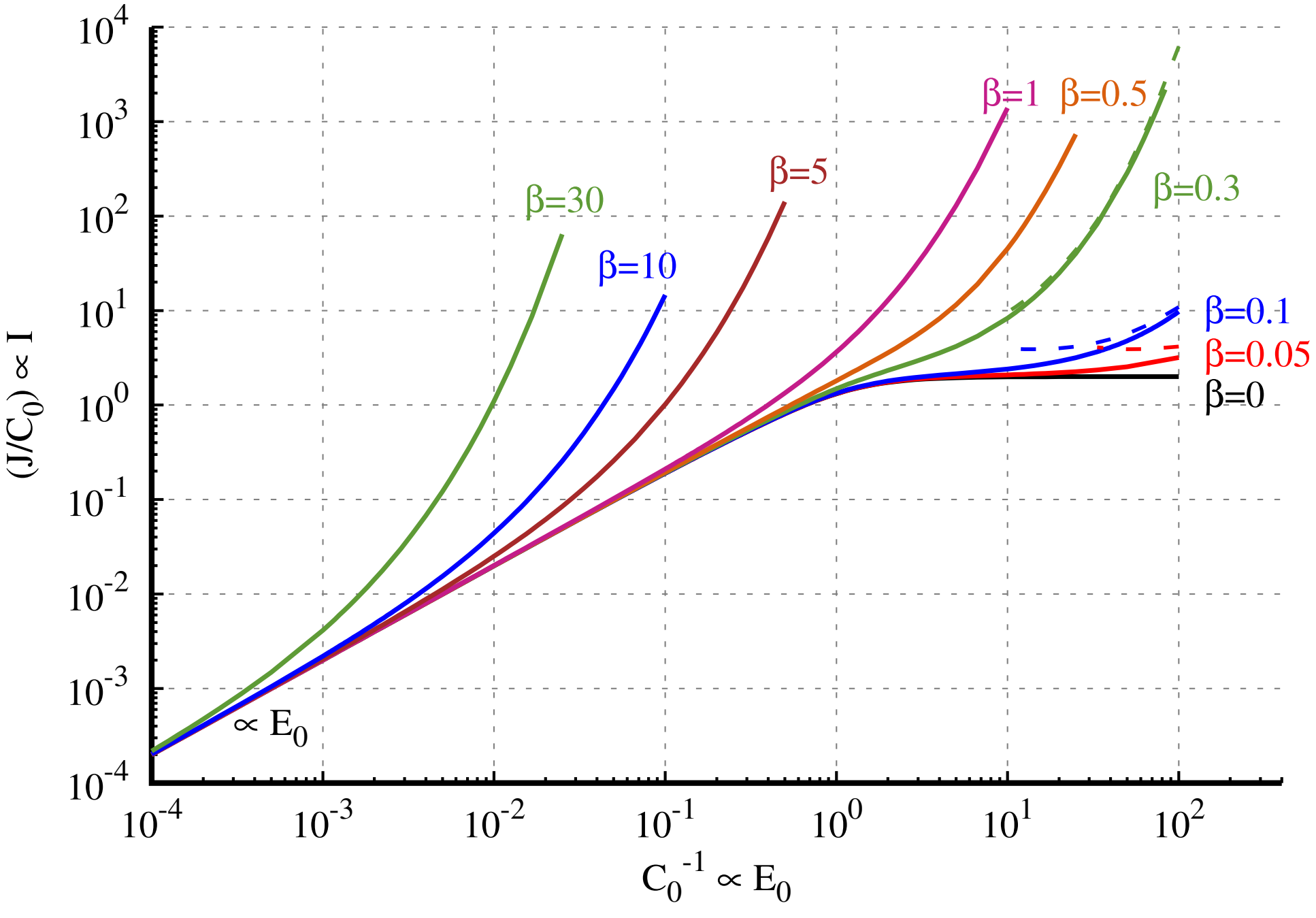
10^4
10^3
10^2
10^1
10^0
10^{-1}
10^{-2}
10^{-3}
10^{-4}
$(J/C_0) \propto I$
β=30
β=10
β=5
β=1
β=0.5
β=0.3
β=0.1
β=0.05
β=0
$\propto E_0$
10^{-4}
10^{-3}
10^{-2}
10^{-1}
10^0
10^1
10^2
$C_0^{-1} \propto E_0$

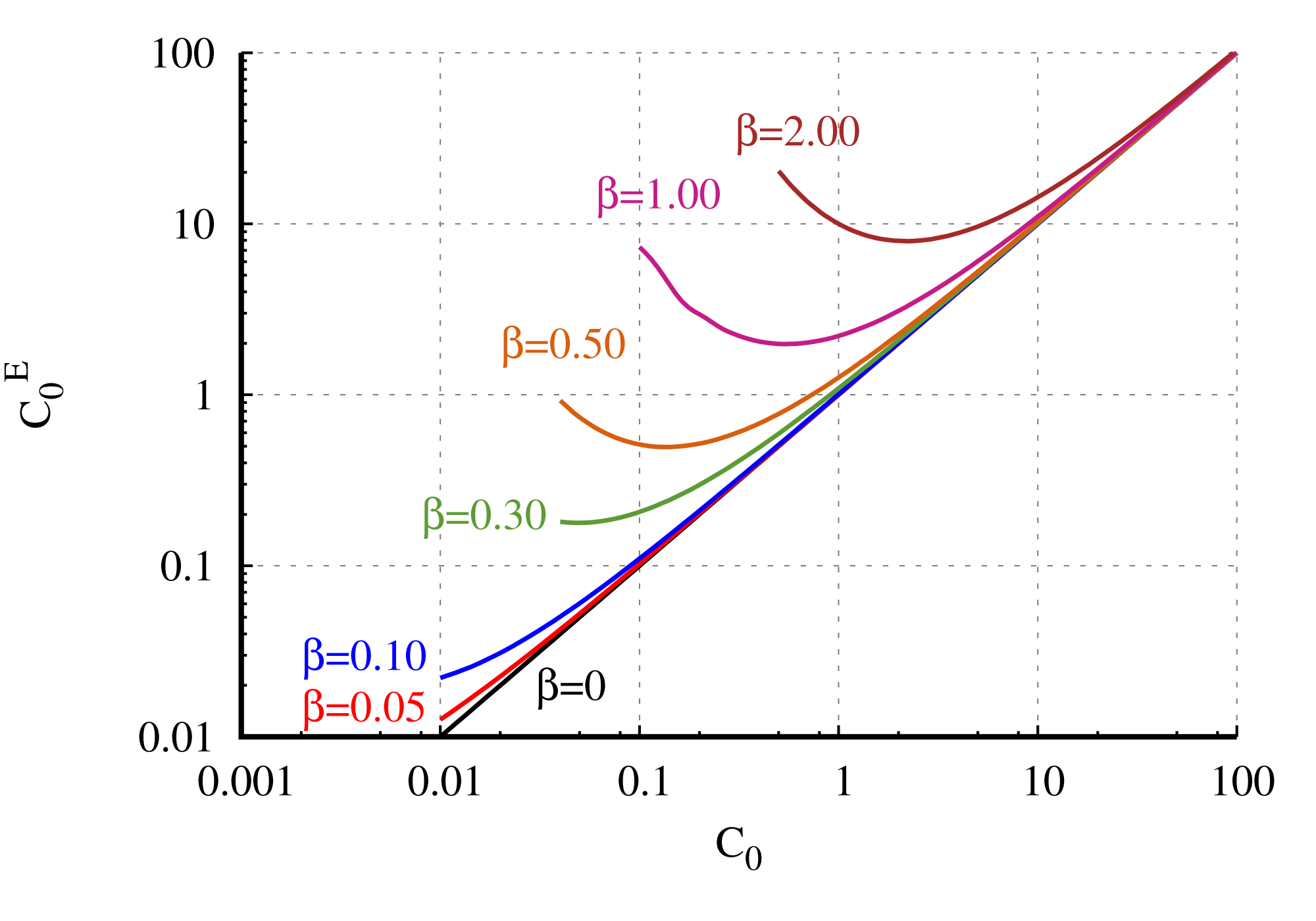
100
10
1
0.1
0.01
0.001
0.01
0.1
1
10
100
C_0^E
C_0
β=2.00
β=1.00
β=0.50
β=0.30
β=0.10
β=0.05
β=0

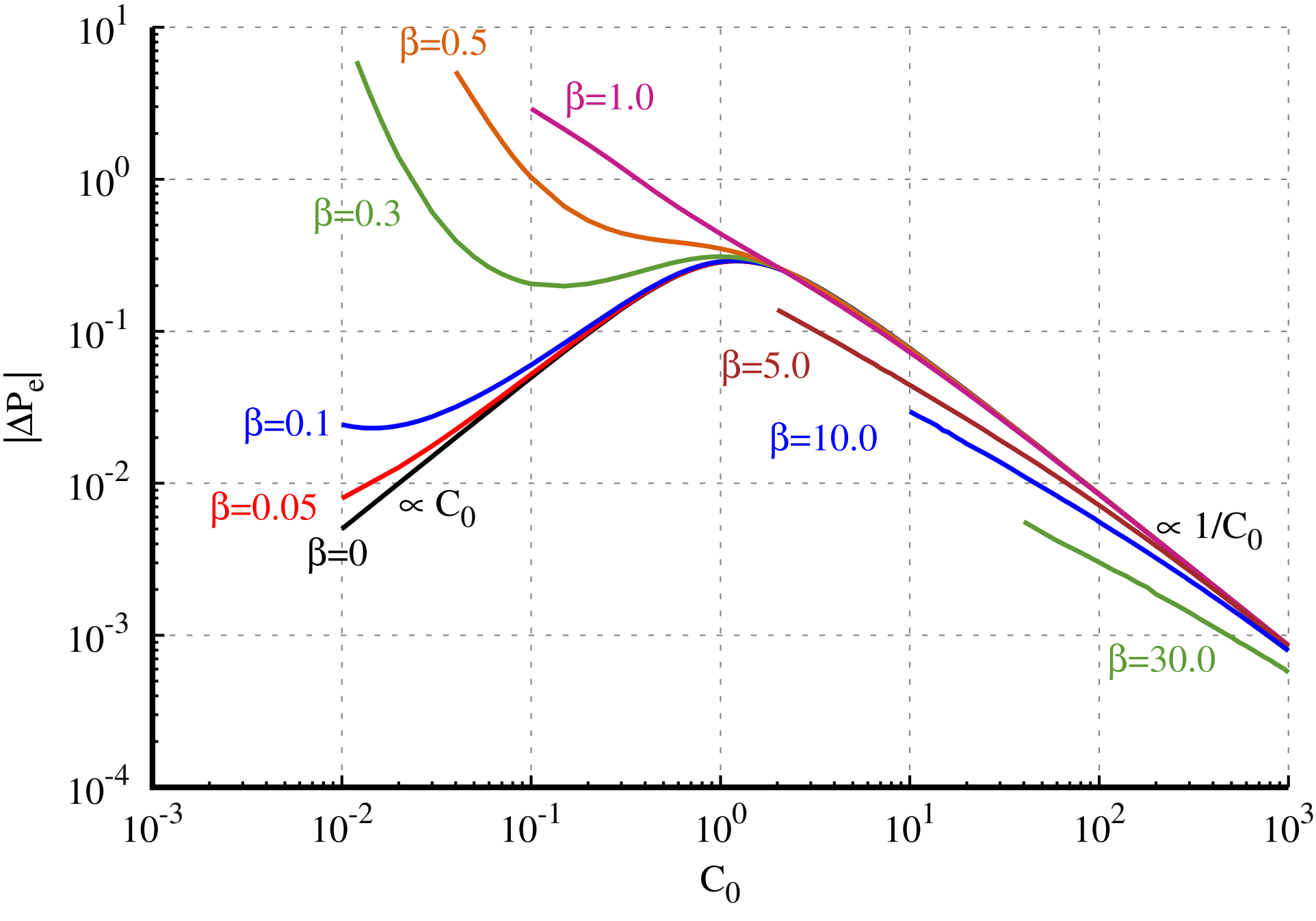
β=0.5
β=1.0
β=0.3
β=5.0
β=0.1
β=10.0
β=0.05
∝ C0
β=0
∝ 1/C0
β=30.0
|ΔPe|
C0
10^1
10^0
10^-1
10^-2
10^-3
10^-4
10^-3
10^-2
10^-1
10^0
10^1
10^2
10^3

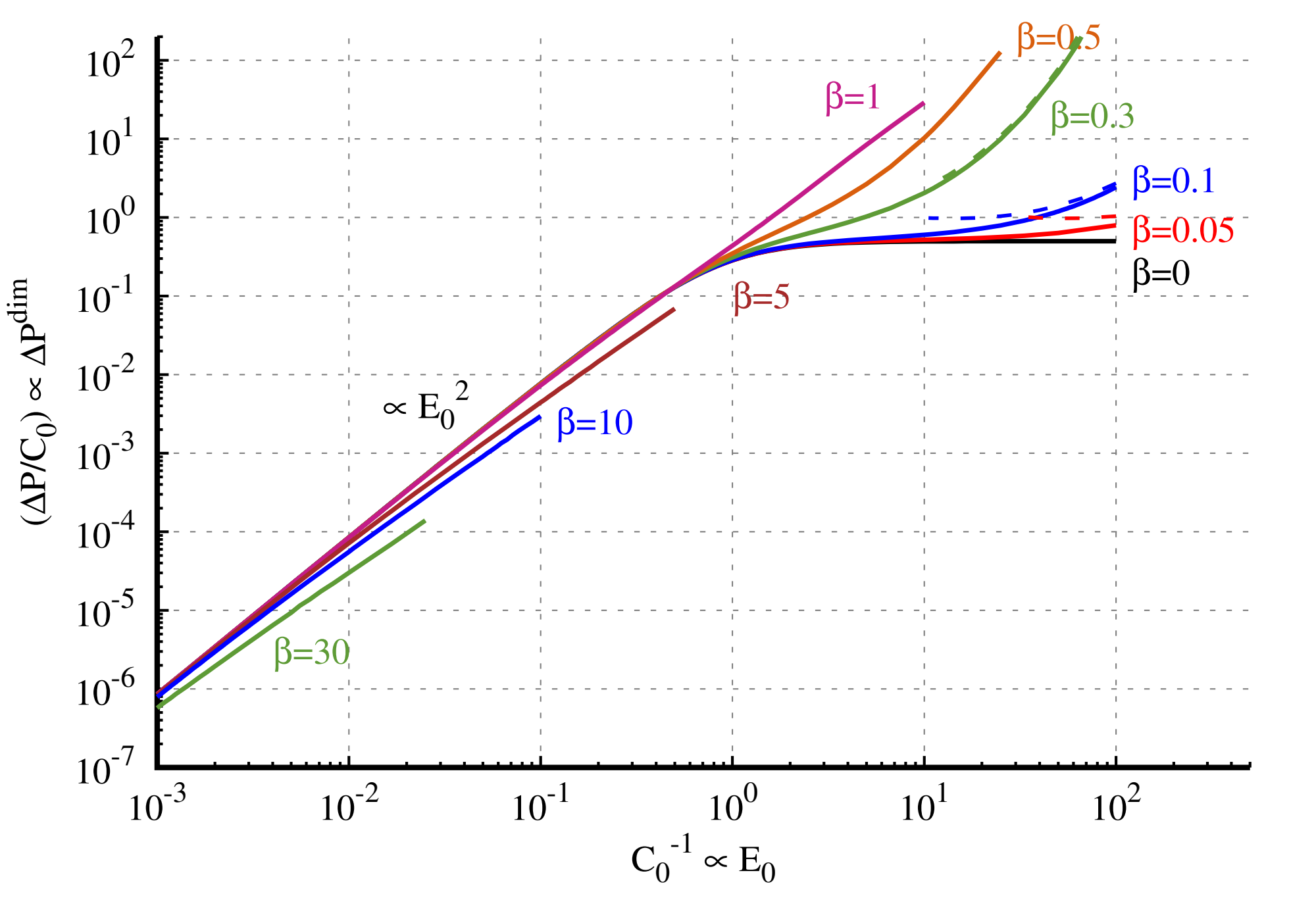
β=0.5
β=1
β=0.3
β=0.1
β=0.05
β=0
β=5
β=10
β=30
∝ E0 2
(ΔP/C0) ∝ ΔPdim
C0 -1 ∝ E0
10-3
10-2
10-1
100
101
102
10-7
10-6
10-5
10-4
10-3
10-2
10-1
100
101
102

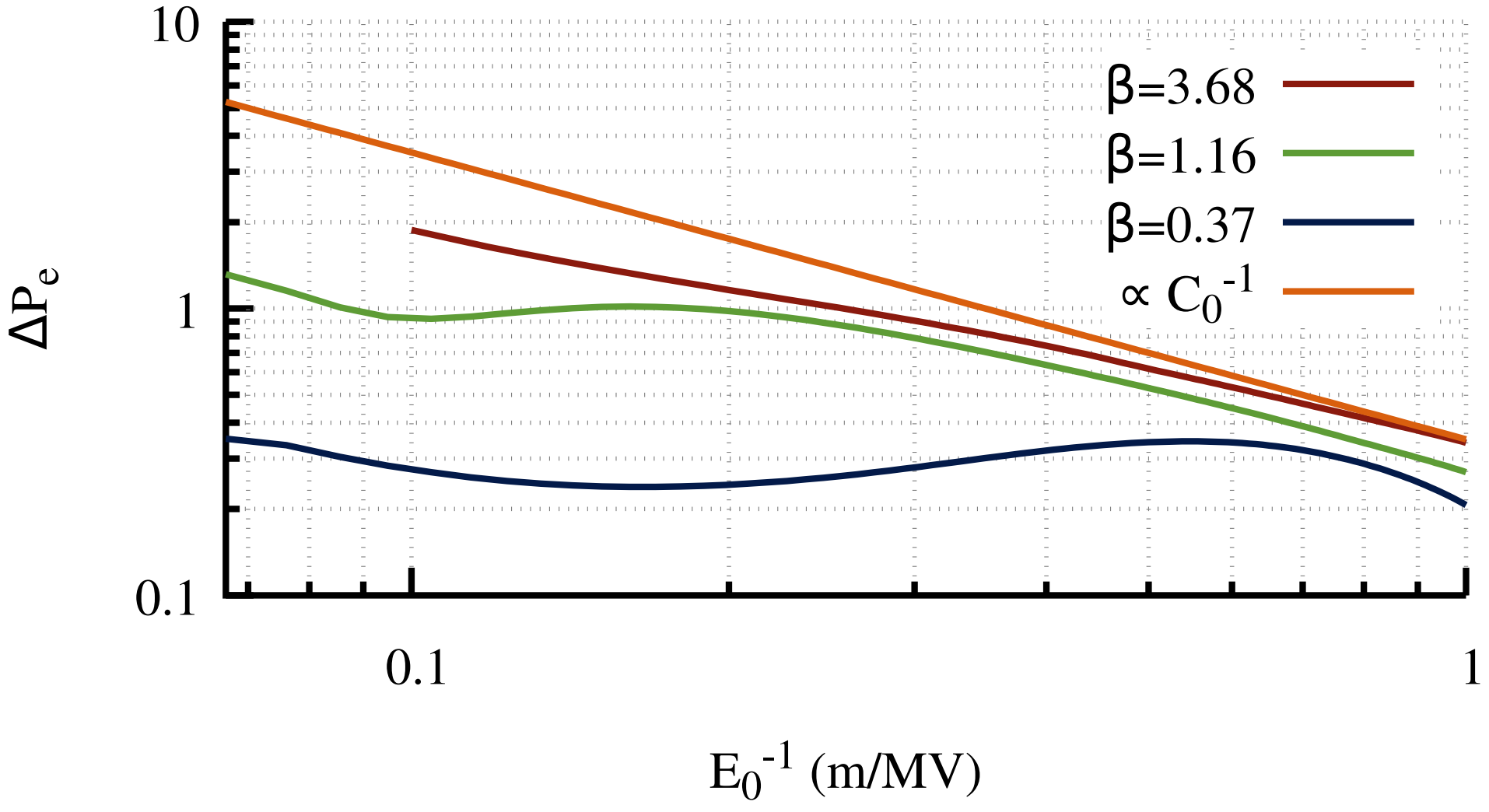
10
1
0.1
ΔP_e
0.1
1
E_0^-1 (m/MV)
β=3.68
β=1.16
β=0.37
∝ C_0^-1